New Phytologist

Check for updates

Coordination of stem and leaf traits define different strategies to regulate water loss and tolerance ranges to aridity

Rosana López[1], Francisco Javier Cano[2], Nicolas K. Martin-StPaul[3], Hervé Cochard[4] and Brendan Choat[2]

[1]Departamento de Sistemas y Recursos Naturales, Universidad Politécnica de Madrid, Madrid 28040, Spain; [2]Hawkesbury Institute for the Environment, Western Sydney University, Locked Bag 1797, Penrith, NSW 2751, Australia; [3]URFM, INRA, Avignon 84000, France; [4]Université Clermont-Auvergne, INRA, PIAF, Clermont-Ferrand 63000, France

Author for correspondence:
Rosana López
Email: rosana.lopez@upm.es

Received: *12 August 2020*
Accepted: *31 December 2020*

New Phytologist (2021) **230:** 497–509
doi: 10.1111/nph.17185

Key words: drought, embolism resistance, intraspecific variation, leaf economic spectrum plant hydraulics, *SurEau* model, tree mortality.

Summary

- Adaptation to drought involves complex interactions of traits that vary within and among species. To date, few data are available to quantify within-species variation in functional traits and they are rarely integrated into mechanistic models to improve predictions of species response to climate change.
- We quantified intraspecific variation in functional traits of two *Hakea* species growing along an aridity gradient in southeastern Australia. Measured traits were later used to parameterise the model *SurEau* to simulate a transplantation experiment to identify the limits of drought tolerance.
- Embolism resistance varied between species but not across populations. Instead, populations adjusted to drier conditions via contrasting sets of trait trade-offs that facilitated homeostasis of plant water status. The species from relatively mesic climate, *Hakea dactyloides*, relied on tight stomatal control whereas the species from xeric climate, *Hakea leucoptera* dramatically increased Huber value and leaf mass per area, while leaf area index (LAI) and epidermal conductance (g_{min}) decreased. With trait variability, *SurEau* predicts the plasticity of LAI and g_{min} buffers the impact of increasing aridity on population persistence.
- Knowledge of within-species variability in multiple drought tolerance traits will be crucial to accurately predict species distributional limits.

Introduction

Ongoing global warming, which is associated with an increased frequency of heat waves and intense droughts, poses an imminent threat to forest function and has the potential to dramatically increase plant mortality (Parmesan, 2006; Choat *et al.*, 2018). One means of prolonging survival in drier conditions is the growth of xylem tissue that is more resistant to embolism (Choat *et al.*, 2018). Accordingly, plants exhibit an enormous range of xylem vulnerabilities to embolism that are directly related to their ecological preferences and with the level of drought stress they experience (Pockman & Sperry, 2000; Choat *et al.*, 2012).

While embolism resistance sets critical thresholds for survival of plants during periods of water stress, several other traits related to drought avoidance such as decreased transpiration rate, increased water acquisition and water storage are crucial in defining desiccation rates and maintaining water potentials within the functional limits of the xylem. Water loss is regulated by leaf area and by stomatal and epidermal conductance. Forest water-use typically scales with leaf area index (LAI) (Specht & Specht, 1989); leaf shedding occurs in many plants during drought to mitigate water stress to the remaining foliage (Martin-StPaul *et al.*, 2013; Rodríguez-Calcerrada *et al.*, 2017) and slow the desiccation rate of the plant (Blackman *et al.*, 2019). The water potential at which leaves lose turgor and stomata close is correlated with drought tolerance (Brodribb *et al.*, 2003; Bartlett *et al.*, 2012). Once the stomata are closed, the residual water loss is largely determined by leakiness from leaf cuticles and incomplete stomatal closure (epidermal conductance). Epidermal conductance has been largely overlooked in studies of drought resistance and its role in predicting drought response remains poorly understood (Duursma *et al.*, 2019). The few available data indicated that trees can reduce epidermal conductance under prolonged water stress (Warren *et al.*, 2011; Cano *et al.*, 2014) according with the high level of plasticity found in a recent meta-analysis (Duursma *et al.*, 2019). At the other end of the hydraulic pathway, deeper root systems offer access to more stable and reliable water sources, allowing plants to maintain more favourable water status and carbon balance during the dry periods or extreme droughts (Nardini *et al.*, 2016). Biomass partitioning to below vs above ground organs and reduction of leaf to sapwood area ratio result in a greater capacity to supply water to the leaves and limit the drop in water potential. Finally, release of water storage during dehydration (capacitance) buffers fluctuations of xylem pressure during transpiration and can contribute to longer desiccation times (Holtta *et al.*, 2009; Meinzer *et al.*, 2009).

© 2021 The Authors
New Phytologist © 2021 New Phytologist Foundation

These traits often vary in a coordinated fashion that is strongly dependent on the environments in which plants grow. Whereas inevitable trade-offs emerge, different associations of traits may succeed in a particular environment and these trade-offs are informative of species ecological strategy (Westoby, 1998; Reich *et al.*, 2003; Reich, 2014). However, most common approaches to studying species range shifts are related to climate niche modelling, yet they can produce ambiguous results as they do not reflect a causal relationship between species distribution and climate (Ay *et al.*, 2017; Journé *et al.*, 2020). Process-based approaches have recently started to incorporate hydraulic traits (Christoffersen *et al.*, 2016; Xu *et al.*, 2016; Powell *et al.*, 2018) but intraspecific patterns of trait variation are barely considered (Rosas *et al.*, 2019). Predictive models that do not incorporate this variation may underestimate or overestimate the potential range shift of species due to climate change (Benito Garzón *et al.*, 2011), or fail when predicting changes in ecosystem functioning and community assembly (Violle *et al.*, 2012).

Trait-based models have proved to be useful tools for synthesising and integrating some of these trait interactions with climate and soil properties in order to determine desiccation dynamics and plant survival during drought (Martin-StPaul *et al.*, 2017; Blackman *et al.*, 2019). The mechanistic model *SurEau*, for example, was developed to simulate the time until complete hydraulic failure and subsequent plant death under severe water stress, by accounting for stomatal and hydraulic traits, plant size and soil conditions (Martin-StPaul *et al.*, 2017). *SurEau* simulates the elementary plant water flow from the soil to the atmosphere due to water potential gradients, and the dynamics of plant water content and embolism formation. The model has recently been improved to consider a dynamic climate and modelling canopy gas exchange (Cochard *et al.*, 2020). *SurEau* assumes that under given climate and soil conditions, the time to hydraulic failure can be view as a two-stage process. The first stage comprises the time between the start of water shortage and stomatal closure. Its duration depends on the rate of transpiration and the water potential causing full stomatal closure (or turgor loss point). The second stage expands from stomatal closure to 100% embolism (death) and it is determined by epidermal conductance, vulnerability to embolism and plant water storage.

Australian plant species provide an excellent opportunity for studies of drought adaptation as the evolutionary history of Australian taxa was uninterrupted by recent glacial periods (Petherick *et al.*, 2013), and populations have not experienced marked bottlenecks or gene flow constraints. Therefore, the adaptation of these lineages to the progressive aridification of the continent over the last 30 Myr has occurred in populations with stable sizes and retained high levels of standing genetic variation (Lamont *et al.*, 2016).

In our study we included populations of two species of *Hakea* across their geographic distribution. The genus *Hakea* is endemic to Australia and is most likely to have had its origin in the Mediterranean biome of SW Australia from where it radiated into a wide range of environments in all of the major biomes (Lamont *et al.*, 2016; Cardillo *et al.*, 2017). We studied *H. leucoptera*, mainly found in arid environments but also occupying Mediterranean, temperate grasslands and tropical savannah, and *H. dactyloides*, which is found in mesic forests closer to the coast. We chose two species of the same genus but growing in contrasting moisture environments to:

(**1**) evaluate how hydraulic traits are coordinated and interact with climate to shape intraspecific drought tolerance;

(**2**) identify key hydraulic traits within species for survival of prolonged or intense droughts;

(**3**) predict whether the current traits shown by each of the studied populations would allow them to survive along an aridity gradient.

For objectives (2) and (3) we evaluated the combined effects of a subset of measured hydraulic traits in objective (1) on survival during drought by using the model *SurEau*. To meet these objectives, we tested the following hypotheses:

(**1**) Leaf and stem traits would be coordinated and the strategy to survive prolonged droughts would differ between the two species. The species from arid sites would follow a conservative growth strategy, showing wider hydraulic safety margins, whereas the species from a temperate climate would follow a fast growing strategy, prioritising carbon gain at the cost of decreasing the hydraulic safety margin.

(**2**) The species growing in drier sites would show higher variability in traits related to regulate water loss, such as LAI, $g_{\min}$ and Ψ_{TLP}, and traits related to withstand more negative water potentials, P_{50} and Huber value (HV), and this variability would correlate with the mean annual precipitation in the place of origin.

(**3**) Populations of both species would be adapted to the environment they grow and the capacity to adapt to drier environments would be limited, particularly in the mesic species.

Materials and Methods

Study sites and plant material

We selected 10 sites covering a broad range of environmental conditions across the distribution of *Hakea leucoptera* R. Br and 4 sites for *Hakea dactyloides* (Gaertn.) Cav. (Fig. 1). For each site, LAI, aridity index (AI), mean annual precipitation (MAP), soil moisture (SMI), mean annual temperature (MAT) and other bioclimatic data were extracted from the *Atlas of Living Australia* (www.ala.org.au). *Hakea leucoptera* populations were located in inland Australia with a climate varying from desert and grassland to temperate and subtropical (Koppen Climate Classification). *Hakea dactyloides* populations were closer to the coast and did not experience a pronounced dry season; three populations were temperate and one subtropical (more details in Table 1, Supporting Information Tables S1, S2).

For each population, eight sun-exposed branches were collected in the field just after dawn during February–March 2016 for leaf pressure–volume analysis, isotopic composition and C and N content. Branches were placed in black plastic bags with wet paper towels to prevent transpiration and kept at 4°C until measured. A second set of 10–20 branches, 1.5–2 m long, was collected during the spring 2016 (September–November), except

© 2021 The Authors
New Phytologist © 2021 New Phytologist Foundation

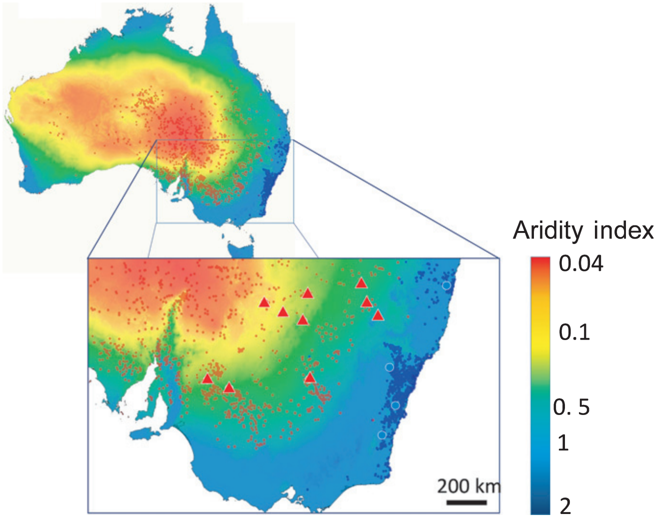

Fig. 1 Natural distribution range of *Hakea leucoptera* (red triangles) and *Hakea dactyloides* (blue dots) across Australia and sampled populations included in this study (bigger dots). Colours represent the aridity index. Data were obtained from the *Atlas of Living Australia* (www.ala.org.au).

for three populations of *H. leucoptera*, Wilcannia, Opal and Tilpa, collected in March 2017.

Native embolism

Native embolism was determined in current-year, 1-yr-old and 2-yr-old segments of five branches per site and species to account for the effect of collection date and water stress from previous years. After releasing tension following Wheeler *et al.* (2013) and Torres-Ruiz *et al.* (2015), initial conductivity (K_h) was measured in 5-cm segments with filtered, degassed 2 mmol KCl solution at low pressure ($\leq$ 4 kPa) with a liquid flowmeter (LiquiFlow L13-AAD-11-K-10S; Bronkhorst, the Netherlands). The segments were then flushed with the same solution at 0.20 MPa for 15 min to remove embolism and subsequently determine maximum hydraulic conductivity (K_{max}). Native loss of conductivity (PLC) was calculated for each segment as:

$$\mathrm{PLC} = 100 \times (1 - K_h/K_{max})$$

Hydraulic safety, hydraulic efficiency and wood density

Xylem vulnerability to embolism curves of 10–12 branches per species and site were measured by the Cavitron technique (Cochard *et al.*, 2005) using a modified bench-top centrifuge (H2100R, Cence Xiangyi, Hunan, China). In the laboratory, branches were recut under water and trimmed to a length of 27.4 cm to fit in the rotor. Leaves distal to this segment were stripped off under water to later calculate the leaf area and leaf mass per area (LMA). The initial conductivity of the segment, K_i, was determined at a xylem pressure of −1.5 MPa in *H. leucoptera* and −0.5 MPa in *H. dactyloides*. The xylem pressure was then lowered stepwise by increasing the rotational velocity, and K_h was again determined while the sample was spinning. The PLC at each pressure step was quantified as $\mathrm{PLC} = 100 \times (1 - K_h/K_i)$ and the xylem pressure was computed at 12, 50 and 88% loss of conductivity (P_{12}, P_{50} and P_{88}, respectively). Embolism resistance curves were corrected for artefactual embolism with the Cavitopen model (López *et al.*, 2018).

The specific hydraulic conductivity (K_s) was calculated by dividing K_i by the xylem cross-sectional area (average distal and proximal xylem area measured with a caliper, subtracting the pith area), and leaf-specific hydraulic conductivity (K_l) as the ratio of K_i to projected leaf area. The projected area of 20 leaves removed from the segments used to construct VCs was obtained with a scanner and analysed with WinFolia (Regent Instruments Inc., Canada). The projected leaf area of *H. leucoptera* was corrected by $\pi/4$ (Lamont *et al.*, 2015). Then leaves were dried at 65°C for 3 d to determine leaf dry mass and LMA. The rest of the leaves were dried and total leaf area was calculated dividing the total leaf mass by LMA. The HV was measured as the ratio of the basal xylem cross-sectional area of the spun segment to the distal projected leaf area supported.

Hydraulic safety margins were calculated as the difference between the turgor loss point (see leaf pressure–volume curves) and P_{50} (HSM_{50}) or P_{88} (HSM_{88}).

Table 1 Characteristics of the 14 populations of *Hakea* included in this study.

Species	Population	Latitude	Longitude	Elevation (m)	LAI	MAT (°C)	MAP (mm)	P_{dry} (mm)	AI	SMI
Hakea leucoptera	Calperum	34.045°S	140.708°E	24	0.5	17.5	246	41	0.19	0.18
	Opal	31.457°S	143.283°E	101	0.3	19.6	255	52	0.10	0.12
	Mildura	34.279°S	142.240°E	34	0.6	17.3	279	50	0.21	0.21
	Wilcannia	31.142°S	144.124°E	83	0.3	19.9	282	57	0.11	0.13
	Toorale	30.103°S	145.609°E	112	0.7	20.3	314	58	0.14	0.16
	Tilpa	31.427°S	144.903°E	140	0.5	19.4	338	71	0.13	0.17
	Binya	34.208°S	146.255°E	155	0.8	16.4	446	97	0.39	0.37
	Kenebri	30.801°S	148.917°E	242	1	18	570	115	0.32	0.33
	Pilliga	30.520°S	148.756°E	170	0.9	18.4	617	112	0.34	0.29
	Dandry	31.149°S	149.363°E	547	1	16.6	774	161	0.47	0.49
H. dactyloides	Monga	35.552°S	149.953°E	750	3.2	12	952	182	0.92	0.74
	Meryla	34.624°S	150.414°E	542	3.9	13.9	1063	217	0.93	0.78
	Blue Mountains	33.572°S	150.361°E	923	3.8	12.8	1183	188	1.10	0.90
	Coffs Harbour	30.038°S	153.007°E	245	3.4	18.2	1288	134	1.05	0.81

AI, aridity index; LAI, leaf area index; MAP, mean annual precipitation; MAT, mean annual temperature; P_{dry}, precipitation of the driest quarter; SMI, soil moisture index.

© 2021 The Authors
New Phytologist © 2021 New Phytologist Foundation

Specific wood density (WD) of the adjacent segment of the spun samples was obtained by dividing the dry weight after drying in an oven at 103°C for 3 d by fresh volume obtained by the water displacement method.

Leaf isotopic composition and C and N content

Fully mature current-year needles were collected at the end of the summer 2016 in the same plants used for hydraulic measurements. They were dried for 3 d at 65°C and finely ground before sending for analysis at the Stable Isotope Facility of the UC Davis (CA, USA). Nitrogen and carbon concentrations and carbon and nitrogen isotope composition ($\delta^{13}C$ and $\delta^{15}N$, respectively) were measured with an elemental analyser (PDZ Europa ANCA-GSL, Sercon Ltd, Cheshire, UK) interfaced to an isotope ratio mass spectrometer (PDZ Europa 20-20; Sercon Ltd).

Leaf pressure–volume curves

The water potential at which leaves lose turgor and parameters of bulk tissue water relations were measured using pressure–volume P–V curves of leaves of a subsample of eight plants per species and population. Small shoots were rehydrated overnight, after which leaves were detached, scanned for projected leaf area and dehydrated slowly on the bench-top (Tyree & Hammel, 1972). Leaf water potential (Ψ_{leaf}), measured with a pressure chamber (PMS Instrument Co., Albany, OR, USA), and leaf mass were assessed at intervals. Leaf dry mass was determined as described before. The saturated water content (SWC) was calculated as the leaf water mass at saturation divided by the dry mass. The relative water content (RWC) of each leaf was calculated as RWC = (fresh weight − dry weight)/(saturated weight − dry weight). The turgor loss point (Ψ_{TLP}) was estimated as the point of transition between curvilinear and linear portions of the graph of $1/\Psi_{leaf}$ vs RWC. The osmotic potential at full turgor (Π_o) was calculated from the intersection between the linear portion of this graph and the *y*-axis. Leaf capacitance was determined using the slope of the P–V curve between full turgor and Ψ_{TLP} (C_{FT}, and $C_{FT}{*}$ when referred to leaf area) and below Ψ_{TLP} (C_{TLP}). The modulus of elasticity at full turgor (ϵ) was defined as the slope of RWC vs pressure potential between full turgor and Ψ_{TLP}.

Epidermal conductance

The epidermal conductance (g_{min}) of detached leaves of the same plants used for P–V curves was estimated by using the rate of water loss. Leaves were recut under distilled water, rehydrated overnight and scanned to determine leaf area. Leaves were then moved to a controlled environment chamber set at 25°C, 50% relative humidity and low light (*c.* 200 µmol) and weighed using a precision balance. They were attached to a 'clothesline' and allowed to dehydrated slowly. Leaves were weighed every 15 min for 3 h and then every hour for 3 h more. The g_{min} was determined from the slope of the linear part of the curve after stomatal closure, and adjusted for temperature and humidity within the chamber.

Embolism resistance curve fitting and statistical analyses

Embolism resistance curves were fitted using a Weibull function and P_{12}, P_{50} and P_{88} were obtained with the FITPLC package (Duursma & Choat, 2017) in R (R Core Team, 2017). The effects of species and population on leaf and stem traits (Table 2) were assessed using nested design analyses of variance with population nested within species. Pearson's correlation coefficients were calculated between climate variables and traits. Bivariate relationships between climate and traits were also assessed using simple linear or nonlinear least squares regression. Three principal component analyses (PCA) were performed with hydraulic stem and leaf traits. In the first one, all traits measured in both species were pooled together. In the other two each species was analysed separately. All variables were equally weighted in the analysis. These analyses were conducted with the software STATISTICA 8 (StatSoft, Tulsa, OK, USA).

Simulations with the *SurEau* model

In order to quantify the relative importance of hydraulic traits in survival of a single plant under extreme droughts, we performed simulations with *SurEau.c* (Cochard *et al.*, 2020. The code to run the program and the MS EXCEL files can be found in Notes S1). This model computes elementary water flow from the soil to the atmosphere accounting for the resistance and the storage of four plant organs, roots, trunk, branches and leaves. Each organ is defined by a symplastic and an apoplastic compartment whose water dynamics to Ψ depends on the P–V curve and the vulnerability to embolism curve, respectively. The flow is driven by the water demand at the leaf stomata level and epidermal level of all organs. After computing the flow, the water content and Ψ of all organs was updated. As soil water content decreases, Ψ_{soil} decreases, causing a decrease of plant water storage and xylem embolism formation, potentially leading to full plant desiccation. The stomatal conductance response to PAR and temperature is modelled following Jarvis *et al.* (1976). The stomatal response to Ψ depends on leaf turgor loss, with full stomatal closure reached at Ψ_{TLP}. In addition, the Farquhar model (Farquhar *et al.*, 1980) was used to compute the gross plant productivity. The elementary computational time step for updating water content and Ψ is low for stability issues (*c.* 0.01s), but climate variations are considered at a hourly time step. Climate variables include temperature, air humidity, atmospheric pressure, global radiation and wind speed.

Despite the complex plant representation in *SurEau*, it is possible to perform a simplified parameterisation as in Cochard *et al.* (2020), by assuming no segmentation between plant organs (i.e. same vulnerability and P–V curves for all organs; Peters *et al.*, 2020). The plant hydraulic conductance was distributed among organs so that 80% of the hydraulic resistance is shared between the roots and the leaves and 20% in the main stem and branches.

Two types of sensitivity analyses were computed. First, we used three measured traits which differed between populations of the same species: LAI, which can be obtained from remote-sensing, Ψ_{tlp}, widely used in drought resistance studies, and g_{min} as emerging trait to explain mortality (Brodribb *et al.*, 2020), all else

© 2021 The Authors
New Phytologist © 2021 New Phytologist Foundation

being constant for each species (see Tables S3–S10), and calculated time to hydraulic failure. Secondly, time to hydraulic failure was calculated using measured values of LAI, Ψ_{tlp} and g_{min} of each population and its relationship with current climate in the origin and other measured traits was assessed using linear least squares regression.

In a second set of simulations, we studied the effect of climate on the performance of each population. We designed a virtual transplantation experiment following an east–west transect (30.25°S 141.25°E to 30.25°S 153.25°E) covering the full range of precipitation for these two species. Daily historical climatic variables were taken from the WATCH-Forcing-Data-ERA-Interim (WFEDI). WFEDI provides daily values at 0.5° spatial resolution for the 1989–2012 period. The daily values were disaggregated at hourly time steps using cosine functions. Along the transect, 25 positions were determined, each spaced 0.5° apart. The *SurEau* model was parameterised with trait values measured for each species and population, including LAI. The model was used to calculate the average seasonal PLC for the period 1950–1975 for each population at each location along the transect.

Finally, for one population of each species (Coffs Harbour and Dandry) we repeated these simulations by gradually decreasing the leaf area to determine the critical leaf area that keeps the embolism rate below a lethal threshold. The impact of this leaf area reduction on the annual cumulative CO_2 assimilation was also calculated.

For all simulations, the water holding capacity of the soil was an important unknown. To focus the study on the role of climate and traits on hydraulic failure, this value was set constant for all populations: same soil texture and volume (1 m^3 per m^2 of soil). This value has been defined by assuming a soil depth of 1 m, which is the average soil depth among sites. In other words, our approach assumes that at all sites and for all populations, fine roots filled out all the soil available. Such a procedure helped to discard the effect of soil water capacity from our analysis.

Results

Native embolism

The degree of native embolism was always low, but some minor variations were observed. PLC was higher in 2-yr-old branch segments (8–19%) than in current-yr growth (<2%) for *H. leucoptera*. Populations from dry areas tended to have slightly higher PLC in 2-yr-old branches than populations from wetter sites (average PLC 11% and 16%, respectively), whereas in *H. dactyloides* native embolism was always lower than 2% (data not shown).

Phenotypic differentiation of functional traits along the climatic gradient

In populations of *H. leucoptera* the AI was positively related with precipitation (MAP), soil moisture (SMI) and negatively with temperature (MAT), showing an association between atmospheric drought and soil drought. As a result, LAI was three times lower in populations from arid sites with lower soil moisture compared with those at wetter sites (Tables 1, S11). For *H. dactyloides*, MAP was partially decoupled from SMI (Table S12) and LAI was similar in all populations (Table 1).

Hakea leucoptera and *H. dactyloides* differed significantly in embolism resistance, WD and water transport efficiency. As expected, the xylem tissue of *H. leucoptera* was more resistant to embolism ($P_{50} = -6.9 \pm 0.2$ MPa in *H. leucoptera* vs $P_{50} = -4.7 \pm 0.1$ MPa in *H. dactyloides*), denser (WD $= 0.689 \pm 0.003$ g cm^{-3} in *H. leucoptera* vs WD $= 0.621 \pm 0.005$ g cm^{-3} in *H. dactyloides*) but less efficient ($K_s = 0.52 \pm 0.03$ kg m^{-1} s^{-1} MPa^{-1} in *H. leucoptera* vs $K_s = 1.37 \pm 0.04$ kg m^{-1} s^{-1} MPa^{-1} in *H. dactyloides*). Within species, however, only WD was negatively correlated with MAP in both species (Fig. 2a). We found little phenotypic differentiation in embolism resistance between populations of the same species (Fig. S1) and variation was not related to MAP (Fig. 2b). In *H. leucoptera*, a three-fold increase in HV with aridity (Fig. 2c) counteracted the decrease of K_s in some populations (Fig. 2d), resulting in K_l not related to MAP (Fig. 2e). Maximum vessel length in *H. leucoptera* decreased with aridity, whereas in *H. dactyloides* was not significantly different between populations (Fig. 2f).

All leaf functional traits, except for $\delta^{15}N$, differed between species (Table S13). Leaves of *H. leucoptera* were more sclerophyllous (LMA $= 771 \pm 5$ g m^{-2} and $\epsilon = 25.5 \pm 0.7$ MPa vs LMA $= 238 \pm 7$ g m^{-2} and $\epsilon = 16.9 \pm 1.1$ MPa in *H. dactyloides*), lost turgor at more negative water potential (-3.6 ± 0.04 MPa vs -2.5 ± 0.06 MPa in *H. dactyloides*) and were more efficient in water use ($\delta^{13}C = -26.6 \pm 0.09$‰ vs $\delta^{13}C = -29.8 \pm 0.13$‰ in *H. dactyloides*). By contrast, leaves of *H. dactyloides* showed lower g_{min} (2.40 ± 0.52 mmol m^{-2} s^{-1} vs 3.72 ± 0.42 mmol m^{-2} s^{-1} in *H. leucoptera*), higher capacitance ($C_{FT} = 0.051 \pm 0.002$ MPa^{-1} and $C_{TLP} = 0.174 \pm 0.008$ MPa^{-1} vs 0.031 ± 0.001 MPa^{-1} and 0.059 ± 0.001 MPa^{-1} in *H. leucoptera* respectively), and higher C : N ratio (69.4 ± 1.3 vs 60.6 ± 0.9 in *H. leucoptera*). The factor population was a significant source of variation in *H. leucoptera* for all leaf traits except for $\delta^{13}C$ (Fig. 3; Table S13). In this species, MAP drove the variation in LMA, g_{min}, SWC, Ψ_{TLP} and Πo (Fig. 3; Table S11). In *H. dactyloides*, MAP was only negatively related to $\delta^{13}C$ (Fig. 3b) and ϵ (Fig. 3e) and positively to C_{FT} (Fig. 3f).

Trade-offs and coordination among functional traits

When all traits from both species are considered together, traits of the leaf economic spectrum, except for LMA, were orthogonal to most hydraulic traits. A single axis of the PCA explained more than 62% of the variance in hydraulic traits (Figs 4, S2). Ψ_{TLP}, Πo and capacitances clustered together and opposite to LMA, ϵ, RWC_{TLP} and $\delta^{13}C$. This axis reflected a trade-off between P_{50}, K_s and WD (Fig. 4a; Table S14) and clearly separated the two species, with *H. dactyloides* having positive coordinates and *H. leucoptera* having negative coordinates (Fig. 4b). The second axis accounted for 20% of the variance and sorted the populations of *H. leucoptera* in two groups, populations with positive coordinates corresponded to mesic sites with higher g_{min} and N

© 2021 The Authors
New Phytologist © 2021 New Phytologist Foundation

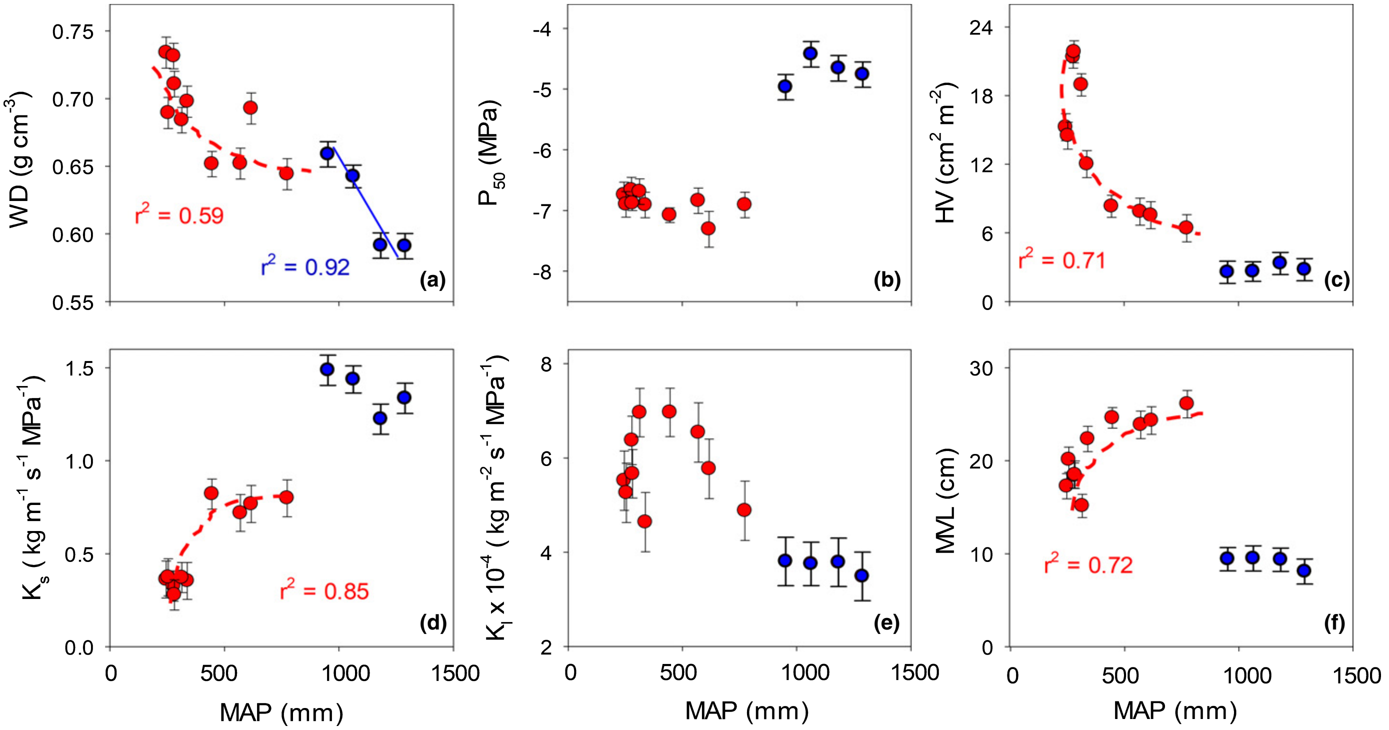

Fig. 2 Variation of stem traits (error bars represent ± SE) of 10 populations of *Hakea leucoptera* (red dots) and four of *H. dactyloides* (blue dots) across a precipitation gradient (MAP, mean annual precipitation). Linear regressions are shown with full lines and nonlinear regressions with dashed lines. Red lines, *H. leucoptera*; blue lines, *H. dactyloides*. (a) Wood density (WD), (b) xylem pressure at 50% loss of conductivity (P_{50}), (c) Huber value (HV), (d) xylem-specific hydraulic conductivity (K_s), (e) leaf-specific conductivity (K_l), and (f) maximum vessel length (MVL).

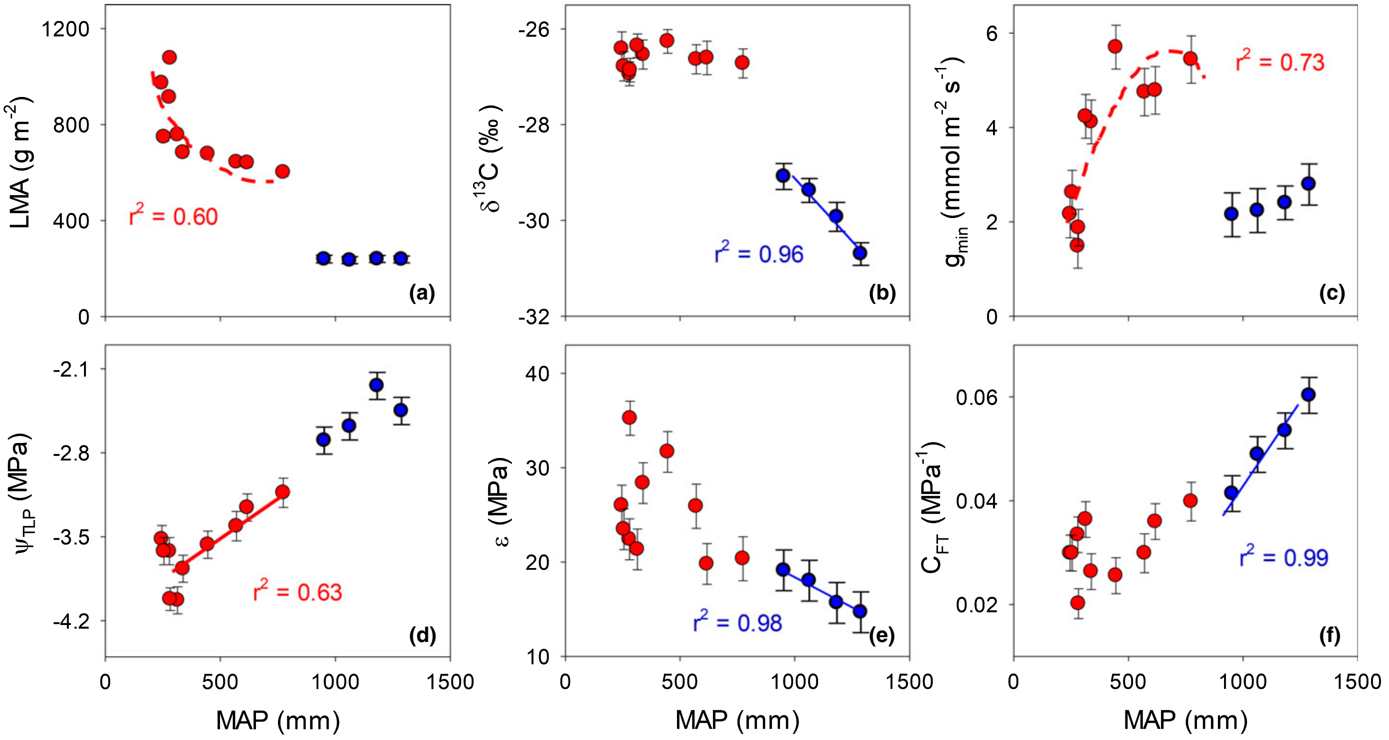

Fig. 3 Variation of leaf traits (error bars represent ± SE) of 10 populations of *Hakea leucoptera* (red dots) and four of *H. dactyloides* (blue dots) across a precipitation gradient (MAP, mean annual precipitation). Linear regressions are shown with full lines and nonlinear regressions with dashed lines. Red lines, *H. leucoptera*; blue lines, *H. dactyloides*. (a) Leaf mass per area (LMA), (b) carbon isotope signature (δ^{13}C), (c) minimum epidermal conductance (g_{min}), (d) turgor loss point (Ψ_{TLP}), (e) leaf modulus of elasticity (ϵ), and (f) capacitance at full turgor (C_{FT}).

© 2021 The Authors
New Phytologist © 2021 New Phytologist Foundation

content, whereas those from drier locations had negative coordinates and were positively related with higher HV and higher C content (Fig. 4b; Table S14). At a lower phylogenetic scale, we observed that coordination of stem and leaf traits was different in each species (Fig. S3). The first axis of the PCA of *H. leucoptera* also showed that higher HV was linked to more sclerophyllous leaves, with lower Ψ_{TLP} and g_{min} and denser wood but less efficient xylem. The second axis reflected the negative correlation between $\delta^{13}C$ and RWC_{TLP} with Ψ_{TLP}, Πo and C_{FT} (Fig. S3a). In *H. dactyloides*, however, Ks, WD and ϵ had positive coordinates in the first axis of the PCA, while g_{min} and capacitances clustered together and had negative coordinates. Unlike in *H. leucoptera*, HV was positively related to Ψ_{TLP}, Πo (Fig. S3b).

Both species displayed positive hydraulic safety margins (HSMs). *Hakea leucoptera* showed HSMs more than 1.5 MPa larger than *H. dactyloides* (Fig. S1). However, HSM_{50} and HSM_{88} of populations of *H. leucoptera* inhabiting mesic sites were slightly higher than those from drier sites (Fig. S4) due to an earlier stomatal closure.

Model *SurEau*- Relative importance of traits determining plant mortality under intense drought

The sensitivity analysis showed that earlier stomatal closure (i.e. less negative Ψ_{TLP}), from −3.6 MPa to −2.4 MPa (33%) in *H. leucoptera* delayed the desiccation time between 18% with g_{min} 1.86 mmol m^{-2} s^{-1} and 11% with g_{min} 5.58 mmol m^{-2} s^{-1} (Fig. 5a). In *H. dactyloides* changes in Ψ_{TLP} from −3.0 MPa to −1.7 MPa (43%) delayed the desiccation time between 26% with g_{min} 1.20 mmol m^{-2} $s^{-1}$and 18% with g_{min} 3.59 mmol m^{-2} s^{-1} (Fig. 5d). Changes in g_{min} in both species impacted more the desiccation time the less negative was Ψ_{TLP} (Fig. 5c,f). In *H. leucoptera*, the desiccation time increased more than 65% changing g_{min} from 5.58 mmol m^{-2} s^{-1} to 1.86 mmol m^{-2} s^{-1} (66%) and *c.* 20% if g_{min} only changed from 5.58 mmol m^{-2} s^{-1} to 3.72 mmol m^{-2} s^{-1} (33%). In *H. dactyloides* changes were more dramatic, and the desiccation time increased by 100% when g_{min} decreased from 3.59 mmol m^{-2} s^{-1} to 1.20 mmol m^{-2} s^{-1} (66%). However, in the range of values of g_{min} measured in the studied populations, changes in the desiccation time were *c.* 28%. In both species LAI had the most impact on desiccation time (Fig. 5b,e). All the rest being equal, decreasing LAI from 1.32 to 0.33 increased the desiccation time between 1.8 and 2.5 times in *H. leucoptera* (Fig. 5b). In *H. dactyloides* changing LAI from 7.15 to 1.8 increased this time by 1.8 (Fig. 5e). These changes were particularly high at

Table 2 List of traits included in the study, with abbreviations and units.

Abbreviation	Trait	Units
Stem traits		
P_{12}	Xylem pressure at 12% loss of hydraulic conductivity	MPa
P_{50}	Xylem pressure at 50% loss of hydraulic conductivity	MPa
P_{88}	Xylem pressure at 88% loss of hydraulic conductivity	MPa
K_s	Xylem-specific conductivity	kg m^{-1} s^{-1} MPa^{-1}
K_l	Leaf-specific conductivity	kg m^{-1} s^{-1} MPa^{-1}
MVL	Maximum vessel length	cm
HV	Huber value	cm^2 m^{-2}
WD	Wood density	g cm^{-3}
Leaf traits		
LMA	Leaf mass per area	g m^{-2}
%C	Carbon content	%
%N	Nitrogen content	%
C : N	Carbon : nitrogen ratio	
$\delta^{13}C$	Carbon isotope signature	‰
$\delta^{15}N$	Nitrogen isotope signature	‰
SWC	Saturated water content	g g^{-1}
RWC_{TLP}	Relative water content at turgor loss point	%
Ψ_{TLP}	Turgor loss point	MPa
Π_o	Osmotic potential at full turgor	MPa
C_{FT}	Capacitance at full turgor	MPa^{-1}
C_{FT}*	Absolute capacitance at full turgor	mol m^{-2} MPa^{-1}
C_{TLP}	Capacitance after turgor loss point	MPa^{-1}
ϵ	Modulus of elasticity	MPa
g_{min}	Minimum epidermal conductance	mmol m^{-2} s^{-1}
Hydraulic safety margins		
HSM_{50}	Hydraulic safety margin at 50% loss of conductivity	MPa
HSM_{88}	Hydraulic safety margin at 88% loss of conductivity	MPa

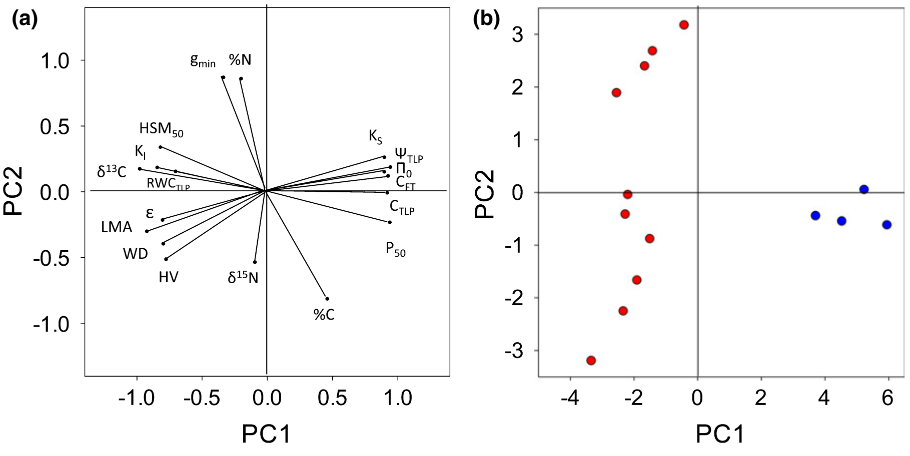

Fig. 4 First two axes of a principal component analysis (PCA) on the relationship between stem and leaf traits. PC1 represents 62% and PC2 20% of the total variation. (a) Correlation coefficients for all variables (acronyms as in Table 2). (b) Population positioning within the multivariate space: in red populations of *Hakea leucoptera*, in blue populations of *H. dactyloides*.

© 2021 The Authors
New Phytologist © 2021 New Phytologist Foundation

lower LAI values, from 0.33 to 0.7 in *H. leucoptera* and from 1.8 to 4 in *H. dactyloides* (Fig. 5b,e). When time to death was simulated with measured values of LAI, Ψ_{TLP}, g_{min} in each population, we found that in populations receiving less than 300 mm of rain in sporadic events (less than 10 d per year with more than 10 mm), with an annual precipitation deficit lower than −170 mm or vapour pressure deficit (VPD) higher than 1.5 kPa, the combination of low LAI and low g_{min} allowed them to survive longer under severe drought (Fig. S5). We also found that other traits, such as high HV and high LMA but low $\mathrm{K_s}$, were correlated with longer survival times (Fig. S6).

Virtual transplantation experiment

The virtual transplantation experiment showed a differential range of loss of hydraulic conductivity among species and populations across the east–west transect (Fig. 6). The PLC of the four populations of *H. dactyloides* dramatically increased when MAP dropped below 820 mm (Fig. 6). The five driest populations of *H. leucoptera* exhibited negligible conductivity loss across the aridity gradient, whereas those inhabiting wetter sites experienced significant loss of conductivity as MAP decreased below certain thresholds, which were in accordance with their current MAP (Fig. 6). This translated for example in 40% loss of conductivity at 145°E and 300 mm MAP of Binya with 446 mm MAP in origin but 70% of Dandry with 774 mm in origin (Fig. 6).

Running the model with variable LAI for one population of each species evidenced that the higher drought resistance of *H. leucoptera* came with a cost in terms of C gain (Fig. S7). In the humid sites of the transect, photosynthesis was three times higher in *H. dactyloides* but decreased at higher rates as MAP decreased and the PLC increased than in *H. leucoptera* (Fig. S7). These simulations with *SurEau* showed that a reduction of leaf area was essential to avoid critical levels of hydraulic failure but came at a cost of a large reduction of photosynthesis. Interestingly, the reduction of leaf area of *H. leucoptera* to thrive at the driest sites was *c.* 50%, in accordance with the observed actual differences among populations of the species (Table 1), which also matched the optimal leaf area for photosynthesis at these sites (Fig. S7).

Discussion

Functional traits represent a powerful approach to understanding species and population responses to abiotic constraints, particularly when they are integrated into mechanistic models. Our results showed that leaf and stem traits conferring drought tolerance were interrelated, but varied independently, allowing different functional trade-offs depending on the phylogenetic scale and the water availability of the species natural range. Increased embolism resistance, higher water-use efficiency, lower leaf area: xylem area ratio (higher HV), and delayed stomatal closure were associated with lower water availability in the native range of *H. leucoptera*, which operates with wider safety margins (Figs 2, 3, S1). Conversely, *H. dactyloides* had lower embolism resistance, and a profligate water-use strategy characterised by lower water-use efficiency, higher LAI and lower HV (Figs 2, 3). Of particular note was the small within-species variability in xylem embolism resistance (Fig. S1), setting a common threshold for hydraulic failure for populations of the same species and suggesting that survival in the drier end of a species range depends on the coordination of drought avoidance traits to maintain water homeostasis. The incorporation of trait variability into mechanistic models such as *SurEau* allows us to identify the limits of drought tolerance and improves our understanding of how coordination and trade-offs in multiple traits contribute to drought survival strategies.

Contrasted strategies to regulate water status

Hakea leucoptera and *H. dactyloides* represent good examples of two well defined strategies of plant water status regulation in response to aridity. At the core of both strategies is Ψ_{TLP}, which delimits the operating range of many species and establishes a threshold of active water loss regulation by the plant (Bartlett *et al.*, 2016). Ψ_{TLP} showed a tight relationship with precipitation or soil moisture (Fig. 3; Tables S11, S12) in agreement with the nearly universal trend across diverse biomes in which water availability is the key defining species' Ψ_{TLP} (Bartlett *et al.*, 2012) and shaping plastic responses within species (Rosas *et al.*, 2019).

Much of the variation we observed in stem and leaf traits aligned along a single axis (Fig. 4), which clearly differentiated between the two species. At one end of the axis, *H. dactyloides* is characterised by high stem hydraulic efficiency, Ψ_{TLP}, Π_{o} and capacitance, consistent with our first hypothesis of a faster growing strategy. Populations of this species, which grows in climates ranging from temperate to subtropical, offset the increase of the water potential gradient with higher water-use efficiency (less negative δ^{13}C), consistent with lower Ψ_{TLP} and observations from many previous studies (Martinez-Vilalta *et al.*, 2009; Aranda *et al.*, 2017). At the other end of the axis, *H. leucoptera* showed characteristics of conservative growth strategy species, with high embolism resistance and HV, low stomatal regulation, and high LMA and ϵ. This combination of traits is commonly found in Australian species inhabiting arid sites where drought tolerance strategies are strongly constrained by low soil water potentials and limited rooting volumes (Mitchell *et al.*, 2008). In other floristically diverse arid ecosystems, several strategies coexist including deep rooting, drought deciduousness or photosynthetic stems (West *et al.*, 2012; Pivovaroff *et al.*, 2014).

Our second hypothesis was partly supported by the results. Except for embolism resistance, *H. leucoptera* showed higher variability in HV and traits related to regulate water loss than *H. dactyloides*. As MAP decreased along the aridity gradient, populations of *H. leucoptera* dramatically increased their HV. This increment in stem area relative to leaf area would act to compensate for the lower branch hydraulic capacity ($\mathrm{K_s}$; Fig. 2) and would help to maintain the water supply to the leaves without the development of excessive pressure drops along the hydraulic pathway (Mencuccini & Grace, 1995; López *et al.*, 2013;

© 2021 The Authors
New Phytologist © 2021 New Phytologist Foundation

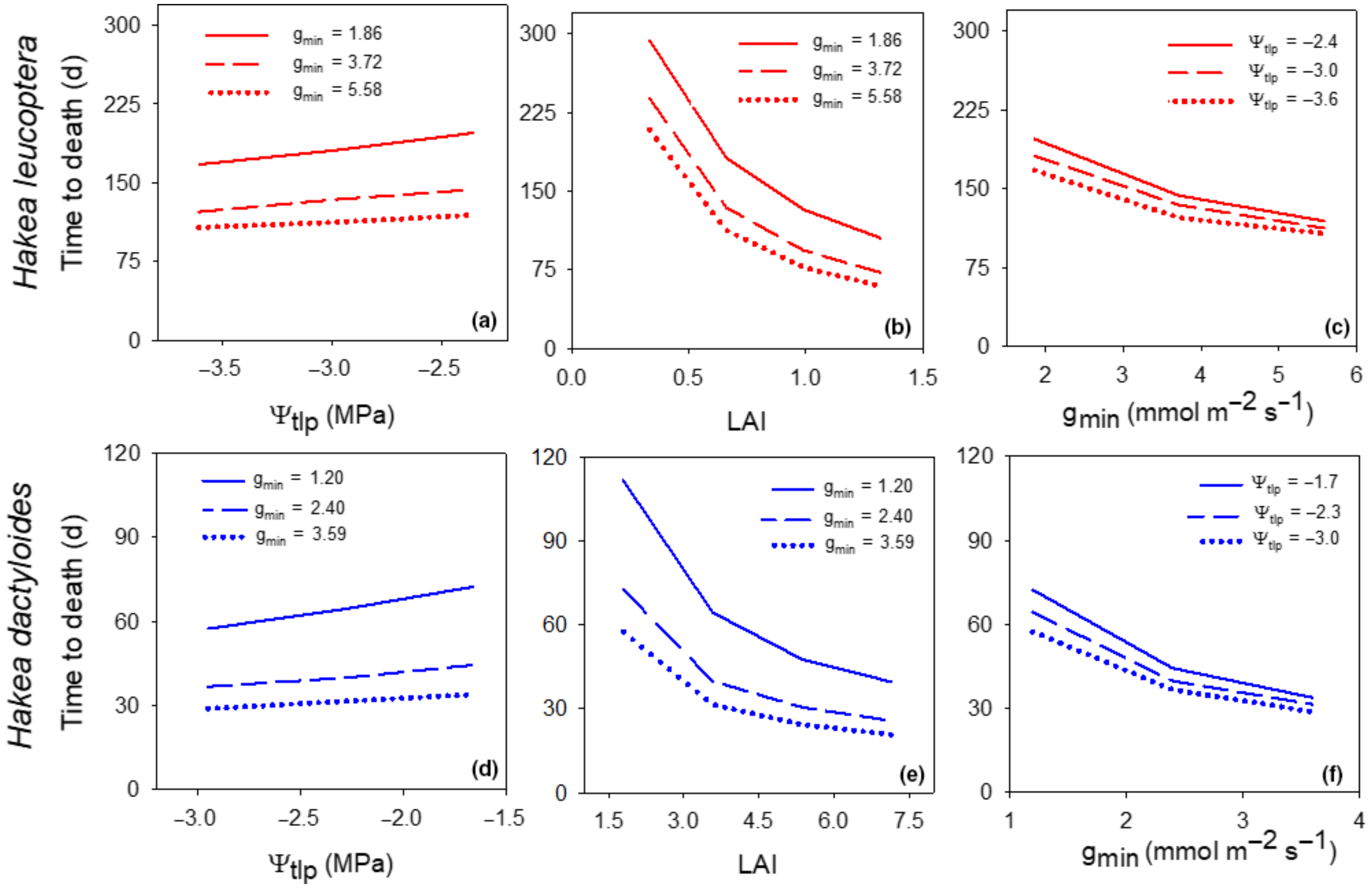

Fig. 5 Simulations with the *SurEau* model of the effect of turgor loss point (Ψ_{TLP}; a, d) and leaf area index (LAI; b, e) and epidermal conductance (g_{min}; c, f) on the time until complete hydraulic failure (time to death) in *Hakea leucoptera* (a–c) and *H. dactyloides* (d–f) at three different rates of epidermal conductance (g_{min}) and turgor loss point (Ψ_{TLP}). The values of Ψ_{TLP}, LAI and g_{min} cover the range measured for each species in populations across a precipitation gradient.

Mencuccini *et al.*, 2019). Lower g_{min} and reduced LAI also allowed populations in dry areas and with sporadic rainfall events to minimise water loss and decrease the rate of desiccation (Fig. S5). Although rates of water loss via the epidermis are extremely low when stomata are closed, over a prolonged period of drought, small differences in g_{min} could result in significant variation in the desiccation time, as shown by simulations with *SurEau* (Fig. 5) and in agreement with lower minimum Ψ in species with more permeable cuticles (Lanning *et al.*, 2020). In a context of climate change, this adaptation capacity will be important not only in areas with decreasing MPA but also in areas where MAP is not predicted to change but precipitation events will become more intense and less frequent, therefore drought periods will be exacerbated (IPCC, 2014).

Coordination and trade-offs

The association between traits reported in our study are in line with recent studies arguing that trait variation is multidimensional (Li *et al.*, 2015; Powell *et al.*, 2017), in which leaf economic, stem economic and plant hydraulic traits are interrelated but vary independently. These different axes of variation allow

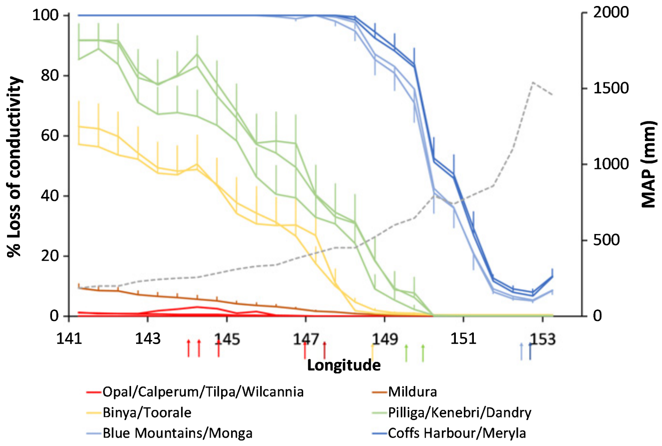

Fig. 6 Predicted loss of hydraulic conductivity (±SE) in a virtual transplantation experiment along a longitudinal transect of four populations of *Hakea dactyloides* (blue lines) and 10 populations of *H. leucoptera*. Soil volume available for each plant was considered constant to 1 m^3. The mean annual precipitation (dashed grey line) observed along the transect is shown for the 1950–1975 period. The in situ location of each site or group of sites along the transect is indicated with a coloured arrow on the *x*-axis.

different functional trait combinations in response to selection and would explain why apparent functional trade-offs in studies across species are not reflected at lower phylogenetic levels.

For example, the significant correlations of P–V curve parameters with LMA (Fig. 4) disappeared within species (Tables S11, S12) revealing that leaf hydraulic parameters are decoupled from the leaf economic spectrum (Wright *et al.*, 2004) at the species level. Although g_{min} formed an independent axis of variation in comparisons among species (Fig. 4; Pivovaroff *et al.*, 2014), in *H. leucoptera*, g_{min} was highly correlated with traits from the leaf economic spectrum, LMA and C and N content (Fig. S3). Leaf mass per unit area, as an index of sclerophylly, is often associated with plants growing under drought-prone conditions and/or nutrient-poor habitats (Lamont *et al.*, 2002). Therefore, sclerophyllous leaves exhibit features characteristic of xeromorphic leaves, such as thicker leaves with thicker cuticles (Groom & Lamont, 1997) which could also decrease epidermal water loss. The higher carbon cost per unit leaf area in terms of leaf and sapwood construction (higher WD) as MAP decreases (Figs 2, 3; Table S11) might confer additional benefits, such as longevity and protection against nutrient, mechanical and herbivory stresses (Groom & Lamont, 1997; Wright & Westoby, 2002; Chave *et al.*, 2009).

While the low variability of vulnerability to embolism within species prevented any inference for the correlation of this trait with other traits, it supports the partial structural decoupling of hydraulic safety and efficiency (Gleason *et al.*, 2016). However, if HV is considered in the context of hydraulic safety by virtue of avoiding high water potential gradients within the plant, a trade-off between safety and efficiency emerges (Fig. S3; Tables S11, S12) as previously reported in species growing in an ecotone between chaparral and desert vegetation in California (Pivovaroff *et al.*, 2016). Additionally, the observed trade-off between hydraulic efficiency and WD in *H. leucoptera* but not in *H. dactyloides* may reflect a constraint of vessel diameter in dry conditions (Pfautsch *et al.*, 2016).

The strong relationship between Ψ_{TLP} and Π_o within and among species (Fig. 4; Tables S11, S12) confirms that Π_o is the major driver of Ψ_{TLP} (Bartlett *et al.*, 2012; Powell *et al.*, 2017), consistent with the role of osmotic adjustment in maintaining cell turgor at low water potentials (Mitchell *et al.*, 2008; López *et al.*, 2009; Bartlett *et al.*, 2012). Tougher leaves (higher ϵ) showed lower capacitance before and after turgor loss (Fig. 4). Leaf capacitance is widely thought to act as a buffer against transient changes in leaf water potential (Sack & Tyree, 2005) but it is unlikely to have any long-term benefits to a plant facing increased desiccation (Blackman & Brodribb, 2011). However, higher ϵ may be necessary during rapid rehydration to sustain cell-wall integrity, to benefit from a lower Π_o (Mitchell *et al.*, 2008) and to maintain the observed nearly constant RWC_{TLP} (Bartlett *et al.*, 2012).

Evidence for local adaptation using a virtual transplantation experiment

In agreement with our third hypothesis, the virtual transplantation experiment showed that *H. dactyloides* would not survive in drier sites due to massive hydraulic failure. Likewise, populations of *H. leucoptera* were well adapted to their current growth environment but were predicted to perform poorly or die at sites drier than their origin (Fig. 6). The nearly universal trend of decreasing LAI with aridity with the concomitant decrease in water use (Limousin *et al.*, 2012; Martin-StPaul *et al.*, 2013) at the cost of decreasing productivity (Rambal *et al.*, 2014) was quantified in this virtual experiment with two populations of *Hakea* (Fig. S7). Notably, the range of the simulated optimal LAI at the driest sites agreed with the actual LAI of the driest populations of *H. leucoptera*. Examples of similar local adaptation in woody species are abundant in the literature (Savolainen *et al.*, 2007; Ramírez-Valiente *et al.*, 2010; López *et al.*, 2013) and highlight the importance of considering species genetic heterogeneity in vegetation models.

Key hydraulic traits for survival under prolonged drought and persistence under future climatic conditions

Choosing specific traits to rapidly screen populations for drought tolerance is challenging. If hydraulic failure is a primary mechanisms linked to mortality (Choat *et al.*, 2018), embolism resistance explains far more of the variation in drought tolerance at the interspecific level (Choat *et al.*, 2012; Lens *et al.*, 2016) compared with the intraspecific level (Martinez-Vilalta *et al.*, 2009; López *et al.*, 2013; Rosas *et al.*, 2019). By integrating different traits within the *SurEau* model, we showed that the effect of three key traits on time to complete hydraulic failure, Ψ_{TLP}, LAI and g_{min} varied between species. In both species LAI significantly impacted the survival time, particularly for lower values of LAI (Fig. 5). Actual measured values of Ψ_{TLP} and g_{min} in *H. dactyloides* affected the rate of dehydration similarly, whereas in *H. leucoptera*, g_{min} had a stronger effect (Fig. 5). Although the simulations within the range of values measured in the field showed that earlier stomatal closure is beneficial for survival, in populations experiencing frequent dry periods, photosynthetic C gain is maintained through a decrease of Ψ_{TLP}. Thus populations show different strategies at the leaf level (stomatal closure at more negative water potential) and the tree level (lower LAI) as aridity increases. These results also highlight the adaptive role of minimising g_{min} in populations experiencing prolonged droughts.

Plants regulate their water status in a highly complex manner involving the coordination of many traits and feedback with environmental conditions. As demonstrated here, there is now great potential to use hydraulic traits to forecast the risk of drought induced mortality in plants across a range of scenarios and predict distributional limits according to water availability. Although drought resistance is dependent on a complex interaction of traits that may change with species, this resistance can be captured with a few key traits and combined in a new generation of hydraulic mechanistic models such as *SurEau*. Certainly many uncertainties still remain in modelling hydraulic failure and predicting mortality risk. We need a deeper knowledge of some aspects such as stomatal dynamics as soil dries, hydraulic segmentation within the plant, proper estimations of rooting volume and water that is available to the plant in the soil or the dynamics of leaf area

© 2021 The Authors
New Phytologist © 2021 New Phytologist Foundation

during drought, which strongly influences LAI. Furthermore, interactions of the individual plant with competition, changes in leaf economics, nutrition and carbon economy deserve further investigation.

Acknowledgements

We thank Jennifer Peters, Markus Nolf and Teresa Rosas for field assistance, Adrián Cano for his patience during field work and Gavin McKenzie for laboratory support. The helpful comments of three anonymous referees improved the clarity and readability of the manuscript. This work was funded by a Marie Curie Fellowship from the EU-FP7 under grant agreement no. IOF-624473. Brendan Choat was supported by an Australian Research Council Future Fellowship (FT130101115).

Author contributions

RL, BC and HC conceived the idea. RL and FJC participated in data collection. RL analysed the experimental data and HC and NKM implemented the *SurEau* model. RL drafted the manuscript with guidance by BC and r/o HC. All authors provided comments to the manuscript.

ORCID

Brendan Choat https://orcid.org/0000-0002-9105-640X
Hervé Cochard https://orcid.org/0000-0002-2727-7072
Francisco Javier Cano https://orcid.org/0000-0001-5720-5865
Rosana López https://orcid.org/0000-0003-3553-9148
Nicolas K. Martin-StPaul https://orcid.org/0000-0001-7574-0108

Ref?er?ences

Aranda I, Bahamonde HA, Sanchez-Gomez D. 2017. Intra-population variability in the drought response of a beech (*Fagus sylvatica* L.) population in the southwest of Europe. *Tree Physiology* **37**: 938–949.

Ay J-S, Guillemot J, Martin-StPaul N, Doyen L, Leadley P. 2017. The economics of land use reveals a selection bias in tree species distribution models. *Global Ecology and Biogeography* **26**: 65–77.

Bartlett MK, Klein T, Jansen S, Choat B, Sack L. 2016. The correlations and sequence of plant stomatal, hydraulic, and wilting responses to drought. *Proceedings of the National Academy of Sciences, USA* **113**: 13098–13103.

Bartlett MK, Scoffoni C, Sack L. 2012. The determinants of leaf turgor loss point and prediction of drought tolerance of species and biomes: a global meta-analysis. *Ecology Letters* **15**: 393–405.

Benito Garzón M, Alía R, Robson TM, Zavala MA. 2011. Intra-specific variability and plasticity influence potential tree species distributions under climate change. *Global Ecology and Biogeography* **20**: 766–778.

Blackman CJ, Brodribb TJ. 2011. Two measures of leaf capacitance: insights into the water transport pathway and hydraulic conductance in leaves. *Functional Plant Biology* **38**: 118–126.

Blackman CJ, Creek D, Maier C, Aspinwall MJ, Drake JE, Pfautsch S, O'Grady A, Delzon S, Medlyn BE, Tissue DT *et al.* 2019. Drought response strategies and hydraulic traits contribute to mechanistic understanding of plant dry-down to hydraulic failure. *Tree Physiology* **39**: 910–924.

Blackman CJ, Li X, Choat B, Rymer PD, De Kauwe MG, Duursma RA, Tissue DT, Medlyn BE. 2019. Desiccation time during drought is highly predictable across species of *Eucalyptus* from contrasting climates. *New Phytologist* **224**: 632–643.

Brodribb TJ, Holbrook NM, Edwards EJ, Gutiérrez MV. 2003. Relations between stomatal closure, leaf turgor and xylem vulnerability in eight tropical dry forest trees. *Plant, Cell & Environment* **26**: 443–450.

Brodribb TJ, Powers J, Cochard H, Choat B. 2020. Hanging by a thread? Forests and drought. *Science* **368**: 261–266.

Cano FJ, López R, Warren CR. 2014. Implications of the mesophyll conductance to CO_2 for photosynthesis and water-use efficiency during long-term water stress and recovery in two contrasting *Eucalyptus* species. *Plant, Cell & Environment* **37**: 2470–2490.

Cardillo M, Weston PH, Reynolds ZKM, Olde PM, Mast AR, Lemmon EM, Lemmon AR, Bromham L. 2017. The phylogeny and biogeography of *Hakea* (*Proteaceae*) reveals the role of biome shifts in a continental plant radiation. *Evolution* **71**: 1928–1943.

Chave J, Coomes D, Jansen S, Lewis SL, Swenson NG, Zanne AE. 2009. Towards a worldwide wood economics spectrum. *Ecology Letters* **12**: 351–366.

Choat B, Brodribb TJ, Brodersen CR, Duursma RA, López R, Medlyn BE. 2018. Triggers of tree mortality under drought. *Nature* **558**: 531–539.

Choat B, Jansen S, Brodribb TJ, Cochard H, Delzon S, Bhaskar R, Bucci SJ, Feild TS, Gleason SM, Hacke UG *et al.* 2012. Global convergence in the vulnerability of forests to drought. *Nature* **491**: 752–755.

Christoffersen BO, Gloor M, Fauset S, Fyllas NM, Galbraith DR, Baker TR, Kruijt B, Rowland L, Fisher RA, Binks OJ. 2016. Linking hydraulic traits to tropical forest function in a size-structured and trait-driven model (TFS v.1-Hydro). *Geoscientific Model Development Discussions* **9**: 4227–4255.

Cochard H, Damour G, Bodet C, Tharwat I, Poirier M, Améglio T. 2005. Evaluation of a new centrifuge technique for rapid generation of xylem vulnerability curves. *Physiologia Plantarum* **124**: 410–418.

Cochard H, Pimont F, Ruffault J, Martin-StPaul N. 2020. *SurEau.c*: a mechanistic model of plant water relations under extreme drought. *bioRxiv*. doi: 10.1101/2020.05.10.086678.

Duursma RA, Blackman CJ, Lopéz R, Martin-StPaul NK, Cochard H, Medlyn BE. 2019. On the minimum leaf conductance: its role in models of plant water use, and ecological and environmental controls. *New Phytologist* **221**: 693–705.

Duursma R, Choat B. 2017. fitplc - an R package to fit hydraulic vulnerability curves. *Journal of Plant Hydraulics* **4**: e002.

Farquhar GD, Von Caemmerer SV, Berry J. 1980. A biochemical model of photosynthetic CO_2 assimilation in leaves of C_3 species. *Planta* **149**: 78–90.

Gleason SM, Westoby M, Jansen S, Choat B, Hacke UG, Pratt RB, Bhaskar R, Brodribb TJ, Bucci SJ, Cao KF *et al.* 2016. Weak tradeoff between xylem safety and xylem-specific hydraulic efficiency across the world's woody plant species. *New Phytologist* **209**: 123–136.

Groom PK, Lamont BB. 1997. Xerophytic implications of increased sclerophylly: interactions with water and light in *Hakea psilorrhyncha* seedlings. *New Phytologist* **136**: 231–237.

Holtta T, Cochard H, Nikinmaa E, Mencuccini M. 2009. Capacitive effect of cavitation in xylem conduits: results from a dynamic model. *Plant, Cell & Environment* **32**: 10–21.

IPCC. 2014. *AR5 synthesis report: climate change 2014.* Geneva, Switzerland: IPCC. [WWW document] URL https://www.ipcc.ch/report/ar5/syr/

Jarvis PG, Monteith JL, Weatherley PE. 1976. The interpretation of the variations in leaf water potential and stomatal conductance found in canopies in the field. *Philosophical Transactions of the Royal Society of London B: Biological Sciences* **273**: 593–610.

Journé V, Barnagaud J-Y, Bernard C, Crochet P-A, Morin X. 2020. Correlative climatic niche models predict real and virtual species distributions equally well. *Ecology* **101**: e02912.

Lamont BB, Groom PK, Cowling RM. 2002. High leaf mass per area of related species assemblages may reflect low rainfall and carbon isotope discrimination rather than low phosphorus and nitrogen concentrations. *Functional Ecology* **16**: 403–412.

Lamont BB, Groom PK, Williams M, He T. 2015. LMA, density and thickness: recognizing different leaf shapes and correcting for their nonlaminarity. *New Phytologist* **207**: 942–947.

Lamont BB, He T, Lim SL. 2016. *Hakea*, the world's most sclerophyllous genus, arose in southwestern Australian heathland and diversified throughout Australia over the past 12 million years. *Australian Journal of Botany* **64**: 77–88.

Lanning M, Wang L, Novick KA. 2020. The importance of cuticular permeance in assessing plant water–use strategies. *Tree Physiology* **40**: 425–432.

Lens F, Picon-Cochard C, Delmas CE, Signarbieux C, Buttler A, Cochard H, Jansen S, Chauvin T, Doria LC, Del Arco M *et al.* 2016. Herbaceous angiosperms are not more vulnerable to drought-induced embolism than angiosperm trees. *Plant Physiology* **172**: 661–667.

Li L, McCormack ML, Ma C, Kong D, Zhang Q, Chen X, Zeng H, Niinemets Ü, Guo D. 2015. Leaf economics and hydraulic traits are decoupled in five species-rich tropical-subtropical forests. *Ecology Letters* **18**: 899–906.

Limousin J-M, Rambal S, Ourcival J-M, Rodríguez-Calcerrada J, Pérez-Ramos IM, Rodríguez-Cortina R, Misson L, Joffre R. 2012. Morphological and phenological shoot plasticity in a Mediterranean evergreen oak facing long-term increased drought. *Oecologia* **169**: 565–577.

López R, López de Heredia U, Collada C, Cano FJ, Emerson BC, Cochard H, Gil L. 2013. Vulnerability to cavitation, hydraulic efficiency, growth and survival in an insular pine (*Pinus canariensis*). *Annals of Botany* **111**: 1167–1179.

López R, Nolf M, Duursma RA, Badel E, Flavel RJ, Cochard H, Choat B. 2018. Mitigating the open vessel artefact in centrifuge-based measurement of embolism resistance. *Tree Physiology* **39**: 143–155.

López R, Rodríguez-Calcerrada J, Gil L. 2009. Physiological and morphological response to water deficit in seedlings of five provenances of *Pinus canariensis*: potential to detect variation in drought-tolerance. *Trees- Structure and Function* **23**: 509–519.

Martinez-Vilalta J, Cochard H, Mencuccini M, Sterck F, Herrero A, Korhonen JF, Llorens P, Nikinmaa E, Nole A, Poyatos R *et al.* 2009. Hydraulic adjustment of Scots pine across Europe. *New Phytologist* **184**: 353–364.

Martin-StPaul N, Delzon S, Cochard H. 2017. Plant resistance to drought depends on timely stomatal closure. *Ecology Letters* **20**: 1437–1447.

Martin-StPaul NK, Limousin JM, Vogt-Schilb H, Rodriguez-Calcerrada J, Rambal S, Longepierre D, Misson L. 2013. The temporal response to drought in a Mediterranean evergreen tree: comparing a regional precipitation gradient and a throughfall exclusion experiment. *Global Change Biology* **19**: 2413–2426.

Meinzer FC, Johnson DM, Lachenbruch B, McCulloh KA, Woodruff DR. 2009. Xylem hydraulic safety margins in woody plants: coordination of stomatal control of xylem tension with hydraulic capacitance. *Functional Ecology* **23**: 922–930.

Mencuccini M, Grace J. 1995. Climate influences the leaf area/sapwood area ratio in Scots pine. *Tree Physiology* **15**: 1–10.

Mencuccini M, Rosas T, Rowland L, Choat B, Cornelissen H, Jansen S, Kramer K, Lapenis A, Manzoni S, Niinemets Ü. 2019. Leaf economics and plant hydraulics drive leaf: wood area ratios. *New Phytologist* **224**: 1544–1556.

Mitchell PJ, Veneklaas EJ, Lambers H, Burgess SS. 2008. Leaf water relations during summer water deficit: differential responses in turgor maintenance and variation in leaf structure among different plant communities in south-western Australia. *Plant, Cell & Environment* **31**: 1791–1802.

Nardini A, Casolo V, Dal Borgo A, Savi T, Stenni B, Bertoncin P, Zini L, McDowell NG. 2016. Rooting depth, water relations and non-structural carbohydrate dynamics in three woody angiosperms differentially affected by an extreme summer drought. *Plant, Cell & Environment* **39**: 618–627.

Parmesan C. 2006. Ecological and evolutionary responses to recent climate change. *Annual Review of Ecology, Evolution, and Systematics* **37**: 637–669.

Peters JMR, Gauthey A, Lopez R, Carins-Murphy MR, Brodribb TJ, Choat B. 2020. Non-invasive imaging reveals convergence in root and stem vulnerability to cavitation across five tree species. *Journal of Experimental Botany* **71**: 6623–6637.

Petherick L, Bostock H, Cohen TJ, Fitzsimmons K, Tibby J, Fletcher M-S, Moss P, Reeves J, Mooney S, Barrows T. 2013. Climatic records over the past 30 ka from temperate Australia–a synthesis from the Oz-INTIMATE workgroup. *Quaternary Science Reviews* **74**: 58–77.

Pfautsch S, Harbusch M, Wesolowski A, Smith R, Macfarlane C, Tjoelker MG, Reich PB, Adams MA. 2016. Climate determines vascular traits in the ecologically diverse genus *Eucalyptus*. *Ecology Letters* **19**: 240–248.

Pivovaroff AL, Pasquini SC, De Guzman ME, Alstad KP, Stemke JS, Santiago LS. 2016. Multiple strategies for drought survival among woody plant species. *Functional Ecology* **30**: 517–526.

Pivovaroff AL, Sack L, Santiago LS. 2014. Coordination of stem and leaf hydraulic conductance in southern California shrubs: a test of the hydraulic segmentation hypothesis. *New Phytologist* **203**: 842–850.

Pockman WT, Sperry JS. 2000. Vulnerability to xylem cavitation and the distribution of Sonoran desert vegetation. *American Journal of Botany* **87**: 1287–1299.

Powell TL, Koven CD, Johnson DJ, Faybishenko B, Fisher RA, Knox RG, McDowell NG, Condit R, Hubbell SP, Wright SJ. 2018. Variation in hydroclimate sustains tropical forest biomass and promotes functional diversity. *New Phytologist* **219**: 932–946.

Powell TL, Wheeler JK, de Oliveira AAR, da Costa ACL, Saleska SR, Meir P, Moorcroft PR. 2017. Differences in xylem and leaf hydraulic traits explain differences in drought tolerance among mature Amazon rainforest trees. *Global Change Biology* **23**: 4280–4293.

R Core Team. 2017. *R: a language and environment for statistical computing*. Vienna, Austria: R Foundation for Statistical Computing. [WWW document] URL https://www.R-project.org/.

Rambal S, Lempereur M, Limousin J, Martin-StPaul N, Ourcival J, Rodríguez-Calcerrada J. 2014. How drought severity constrains gross primary production (GPP) and its partitioning among carbon pools in a *Quercus ilex* coppice? *Biogeosciences* **11**: 6855–6869.

Ramírez-Valiente JA, Sánchez-Gómez D, Aranda I, Valladares F. 2010. Phenotypic plasticity and local adaptation in leaf ecophysiological traits of 13 contrasting cork oak populations under different water availabilities. *Tree Physiology* **30**: 618–627.

Reich PB. 2014. The world-wide 'fast–slow'plant economics spectrum: a traits manifesto. *Journal of Ecology* **102**: 275–301.

Reich PB, Wright I, Cavender-Bares J, Craine J, Oleksyn J, Westoby M, Walters M. 2003. The evolution of plant functional variation: traits, spectra, and strategies. *International Journal of Plant Sciences* **164**(S3): S143–S164.

Rodríguez-Calcerrada J, Li M, López R, Cano FJ, Oleksyn J, Atkin OK, Pita P, Aranda I, Gil L. 2017. Drought-induced shoot dieback starts with massive root xylem embolism and variable depletion of nonstructural carbohydrates in seedlings of two tree species. *New Phytologist* **213**: 597–610.

Rosas T, Mencuccini M, Barba J, Cochard H, Saura-Mas S, Martínez-Vilalta J. 2019. Adjustments and coordination of hydraulic, leaf and stem traits along a water availability gradient. *New Phytologist* **223**: 632–646.

Sack L, Tyree MT. 2005. Leaf hydraulics and its implications in plant structure and function. *Vascular transport in plants*. San Diego, CA, USA: Elsevier, 93–114.

Savolainen O, Pyhäjärvi T, Knürr T. 2007. Gene flow and local adaptation in trees. *Annual Review of Ecology, Evolution, and Systematics* **38**: 595–619.

Specht R, Specht A. 1989. Canopy structure in Eucalyptus-dominated communities in Australia along climatic gradients. *Acta oecologica. Oecologia plantarum* **10**: 191–213.

Torres-Ruiz JM, Jansen S, Choat B, McElrone AJ, Cochard H, Brodribb TJ, Badel E, Burlett R, Bouche PS, Brodersen CR. 2015. Direct X-ray microtomography observation confirms the induction of embolism upon xylem cutting under tension. *Plant Physiology* **167**: 40–43.

Tyree M, Hammel H. 1972. The measurement of the turgor pressure and the water relations of plants by the pressure-bomb technique. *Journal of Experimental Botany* **23**: 267–282.

Violle C, Enquist BJ, McGill BJ, Jiang L, Albert CH, Hulshof C, Jung V, Messier J. 2012. The return of the variance: intraspecific variability in community ecology. *Trends in ecology & evolution* **27**: 244–252.

Warren CR, Aranda I, Cano FJ. 2011. Responses to water stress of gas exchange and metabolites in *Eucalyptus* and *Acacia* spp. *Plant, Cell & Environment* **34**: 1609–1629.

West AG, Dawson TE, February EC, Midgley GF, Bond WJ, Aston TL. 2012. Diverse functional responses to drought in a Mediterranean-type shrubland in South Africa. *New Phytologist* **195**: 396–407.

Westoby M. 1998. The relationship between local and regional diversity: comment. *Ecology* **79**: 1825–1827.

© 2021 The Authors
New Phytologist © 2021 New Phytologist Foundation

Wheeler JK, Huggett BA, Tofte AN, Rockwell FE, Holbrook NM. 2013. Cutting xylem under tension or supersaturated with gas can generate PLC and the appearance of rapid recovery from embolism. *Plant, Cell & Environment* 36: 1938–1949.

Wright IJ, Reich PB, Westoby M, Ackerly DD, Baruch Z, Bongers F, Cavender-Bares J, Chapin T, Cornelissen JH, Diemer M. 2004. The worldwide leaf economics spectrum. *Nature* 428: 821.

Wright IJ, Westoby M. 2002. Leaves at low versus high rainfall: coordination of structure, lifespan and physiology. *New Phytologist* 155: 403–416.

Xu X, Medvigy D, Powers JS, Becknell JM, Guan K. 2016. Diversity in plant hydraulic traits explains seasonal and inter-annual variations of vegetation dynamics in seasonally dry tropical forests. *New Phytologist* 212: 80–95.

Supporting Information

Additional Supporting Information may be found online in the Supporting Information section at the end of the article.

Fig. S1 Embolism resistance curves and hydraulic safety margins.

Fig. S2 Scree plot of the PCA of stem and leaf hydraulic traits.

Fig. S3 PCA of stem and leaf hydraulic traits measured in *Hakea leucoptera* and *Hakea dactyloides*.

Fig. S4 Relationship between embolism resistance and turgor loss point.

Fig. S5 Relationship between climatic variables and time until complete hydraulic failure.

Fig. S6 Relationship between measured traits and time until complete hydraulic failure.

Fig S7 Loss of hydraulic conductivity and photosynthesis in a virtual transplantation experiment.

Notes S1 Zip file with the c code to run the simulations with *SurEau*; MS EXCEL file with the different traits for all the sites and the climatic conditions for each site and two .ini files to run the program.

Table S1 Stand and soil characteristics of the populations of *Hakea* included in the study.

Table S2 Bioclimatic variables of the populations of *Hakea* included in the study.

Table S3 Physiological parameters of *H. leucoptera* used in the sensitivity analysis with *SurEau*.

Table S4 Climate parameters of *H. leucoptera* used in the sensitivity analysis with *SurEau*.

Table S5 Parameters for the flows in gas phase of *H. leucoptera* used in the sensitivity analysis with *SurEau*.

Table S6 Soil parameters of *H. leucoptera* used in the sensitivity analysis with *SurEau*.

Table S7 Physiological parameters of *H. dactyloides* used in the sensitivity analysis with *SurEau*.

Table S8 Climate parameters of *H. dactyloides* used in the sensitivity analysis with *SurEau*.

Table S9 Parameters for the flows in gas phase of *H. dactyloides* used in the sensitivity analysis with *SurEau*.

Table S10 Soil parameters of *H. dactyloides* used in the sensitivity analysis with *SurEau*.

Table S11 Correlation matrix of climatic variables and traits included in the study for 10 populations of *H. leucoptera*.

Table S12 Correlation matrix of climatic variables and traits included in the study for 10 populations of *H. dactyloides*.

Table S13 Explained variation by factors species and populations.

Table S14 Loadings of the stem and leaf traits on the PCA.

Please note: Wiley Blackwell are not responsible for the content or functionality of any Supporting Information supplied by the authors. Any queries (other than missing material) should be directed to the *New Phytologist* Central Office.

© 2021 The Authors
New Phytologist © 2021 New Phytologist Foundation

***New Phytologist* Supporting Information**

Article title: Coordination of stem and leaf traits define different strategies to regulate water loss and tolerance ranges to aridity
Authors: Rosana López, Francisco Javier Cano, Nicolas K Martin-StPaul, Hervé Cochard, Brendan Choat
Article acceptance date: 31 December 2020

The following Supporting Information is available for this article:

Parameters for simulations with SurEau (Tables S3-S10)

Table S8. Climate parameters of *H. dactyloides* used in the sensitivity analysis with *SurEau*

Table S9. Parameters for the flows in gas phase of *H. dactyloides* used in the sensitivity analysis with *SurEau*

Table S10. Soil parameters of *H. dactyloides* used in the sensitivity analysis with *SurEau*

Table S11 Correlation matrix of climatic variables and traits included in the study for 10 populations of *H. leucoptera*

Table S12 Correlation matrix of climatic variables and traits included in the study for 4 populations of *H. dactyloides*

Table S13 Explained variation by factors species and populations.

Table S14. Loadings of the stem and leaf traits on the PCA.

Notes S1. Zip file with the c code to run the simulations with *SurEau*; Excel file with the different traits for all the sites and the climatic conditions for each site and two .ini files to run the program.

Figure S1. Average embolism resistance curves and average hydraulic safety margins (HSM88) for ten populations of *H. leucoptera* (red) and four populations H. *dactyloides* (blue). Embolism resistance curves for each population are shown in lighter colors.

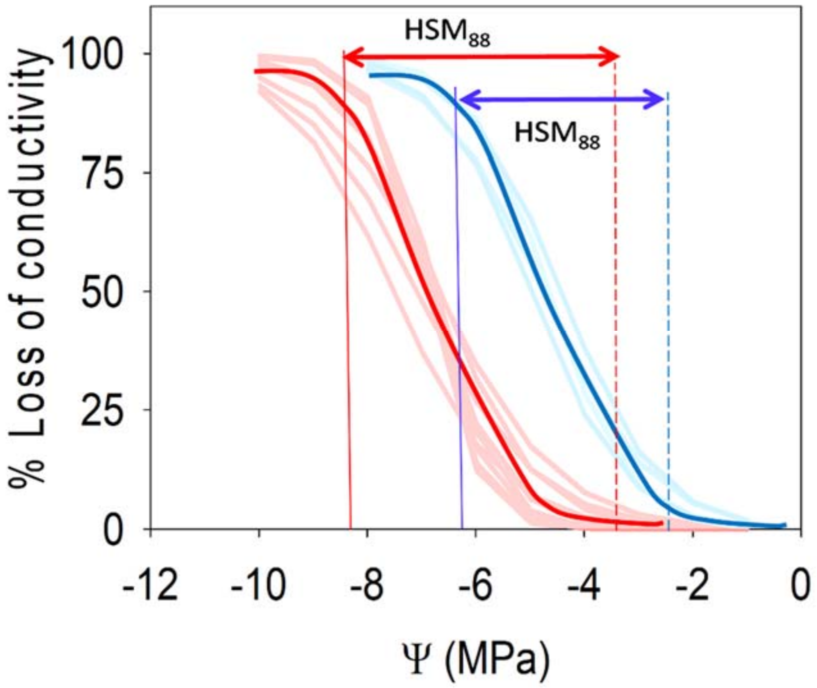

Figure S2. Scree plot of the Principal Component Analysis (PCA) of stem and leaf hydraulic traits measured in ten populations of *H. leucoptera* and four populations *H. dactyloides*. All variables were equally weighted in the analysis.

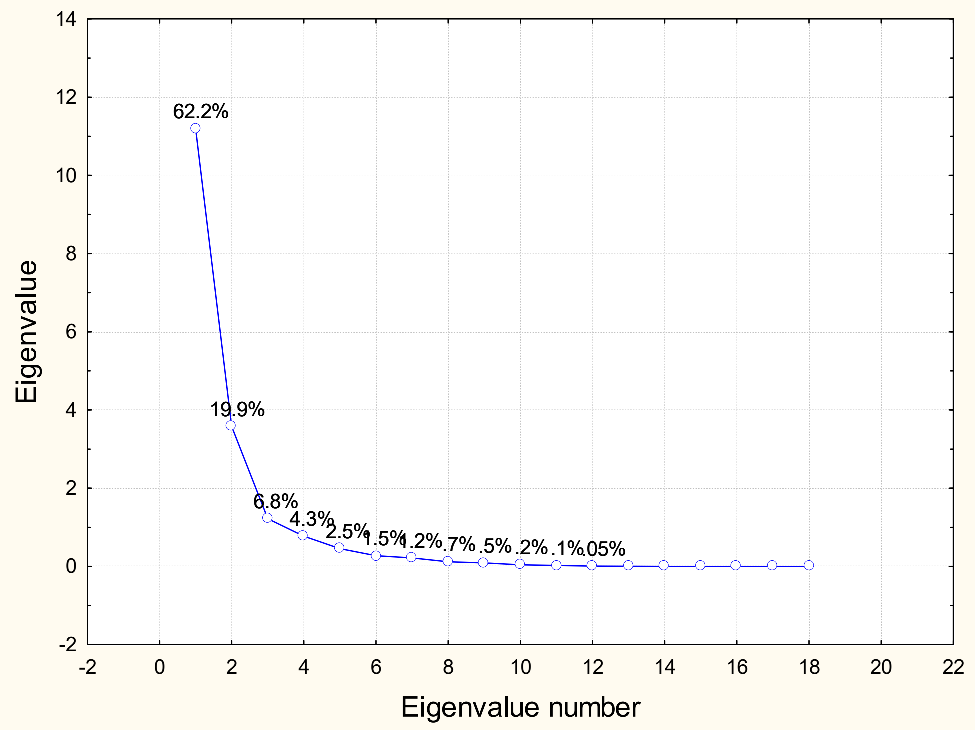

Figure S3. First two axes of a Principal Component Analysis (PCA) on the relationship between stem and leaf traits. (a) Correlation coefficients for all variables measured in populations of *H. leucoptera*. (b) Correlation coefficients for all variables measured in populations of *H. dactyloides*. Acronyms as in Table 2.

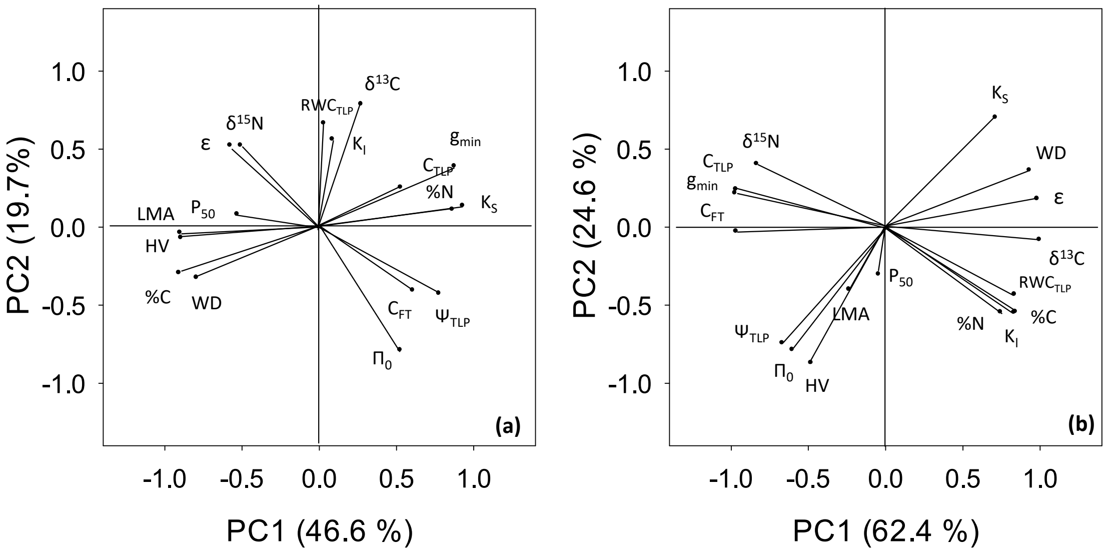

Figure S4. Relationship between embolism resistance and turgor loss point in ten populations of *H. leucoptera* (red dots) and four populations of *H. dactyloides* (blue dots). The safety margin (HSM_{50}) is the distance between each point and the 1:1 (dashed) line. Values are means ±SE.

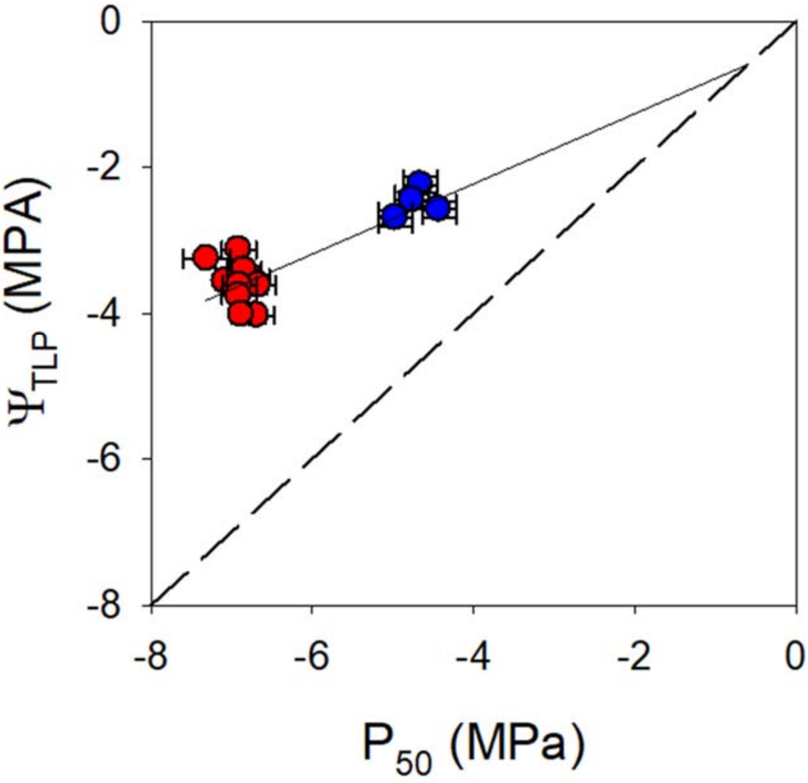

Figure S5. Relationship between current local climatic variables (a-f) of 10 populations of *H. leucoptera* (red dots) and 4 of *H. dactyloides* (blue dots) and time until complete hydraulic failure (time to death) simulated with the model *SurEau* using values of LAI, Ψ_{TLP}, and g_{min} measured in each population. (a) mean annual precipitation (MAP), (b) number of days with rain, (c) aridity index (AI), (d) number of days with rain higher than 10 mm, (e) annual precipitation deficit, (f) Maximum month vapour pressure deficit (VPD).

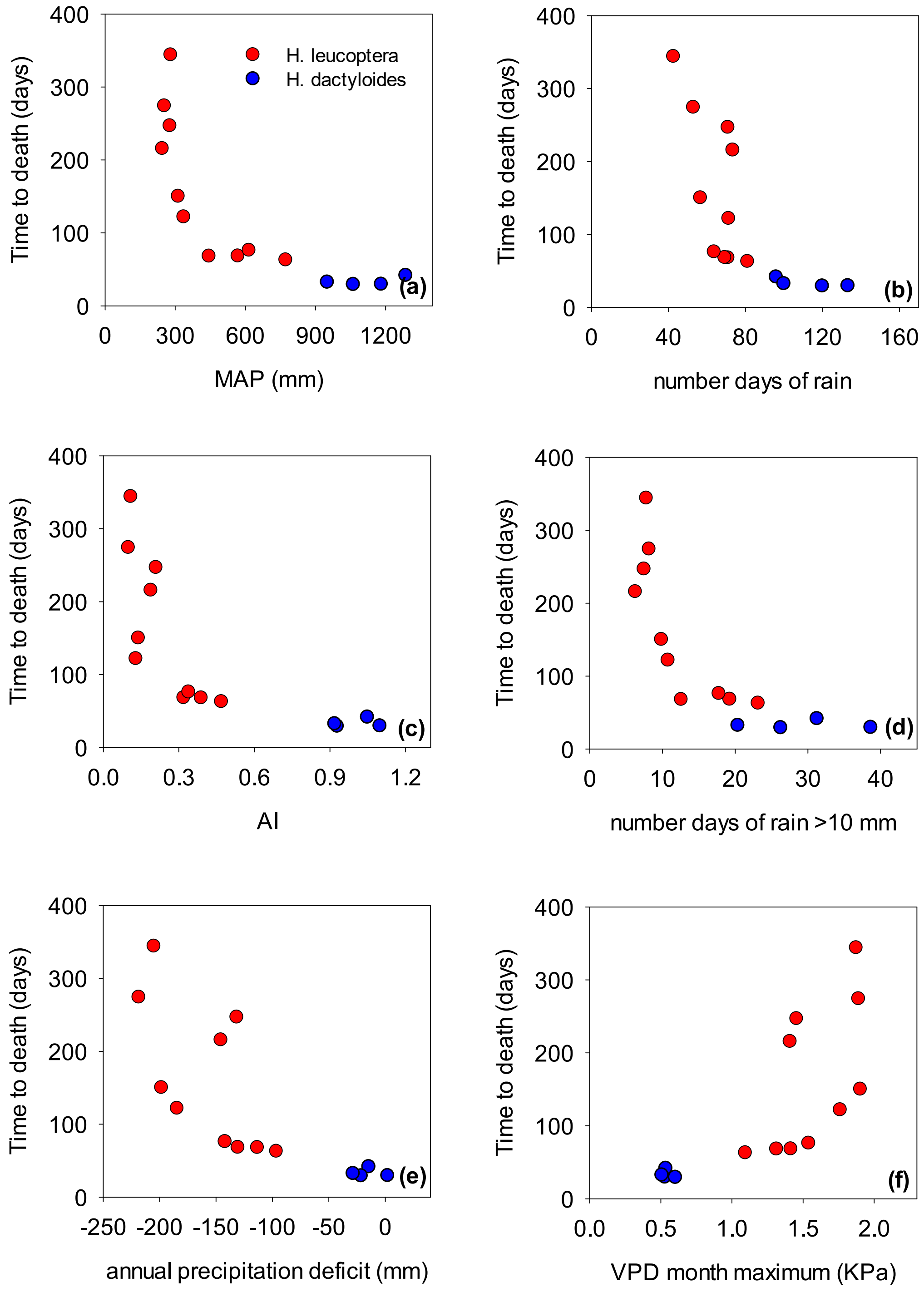

Figure S6. Relationships between (a) Huber value (HV), (b) leaf area index (LAI), (c) minimum conductance (g_{min}), (d) turgor loss point (Ψ_{TLP}), (e) leaf mass per area (LMA), (f) specific hydraulic conductivity (Ks) of 10 populations of *H. leucoptera* (red dots) and 4 of *H. dactyloides* (blue dots) and time until complete hydraulic failure (time to death) simulated with the model *SurEau* using values of LAI, Ψ_{TLP}, and g_{min} measured in each population. Note that HV, LMA and Ks are also the values measured in each populations but these parameters are not included in the model.

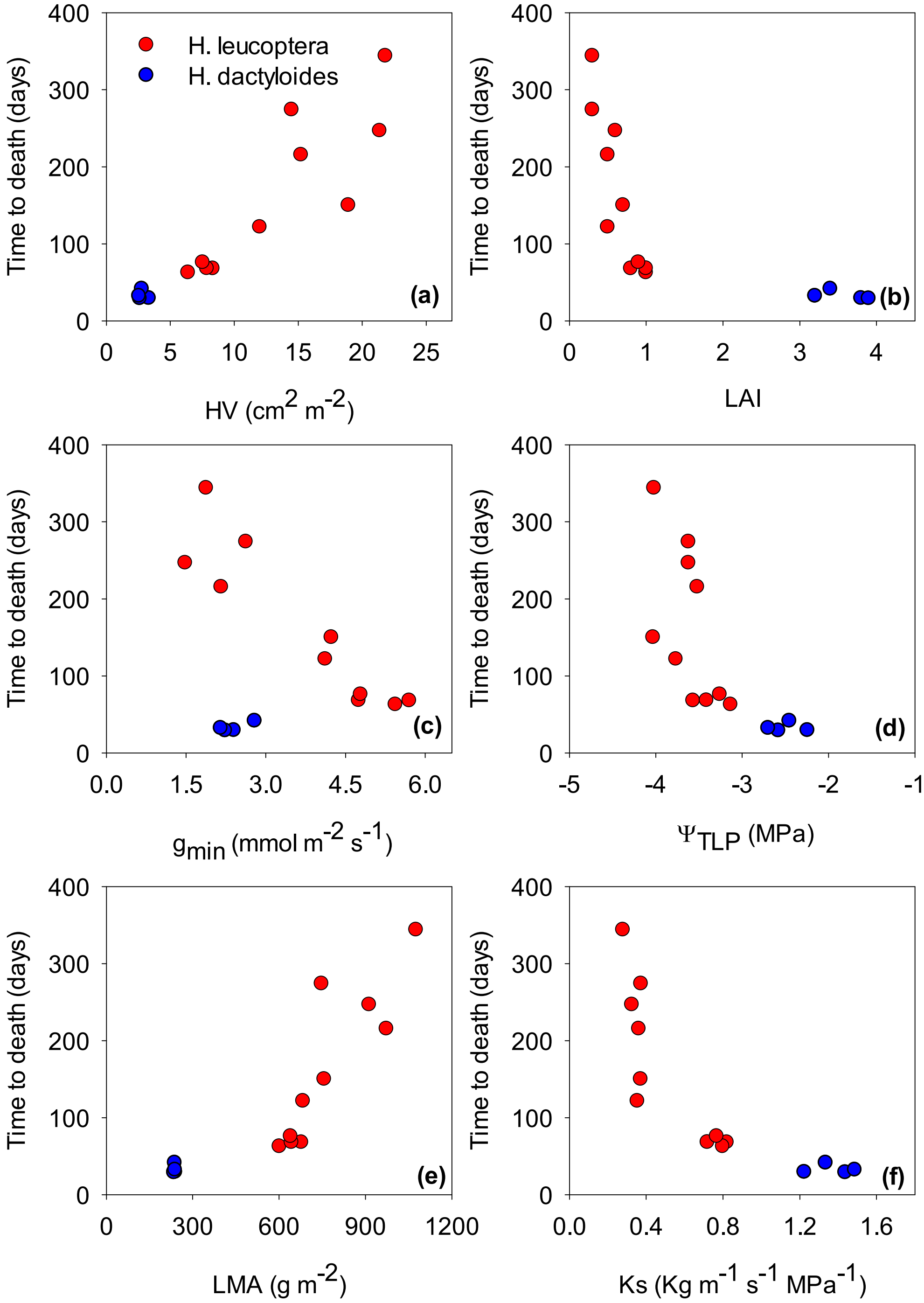

Figure S7. Loss of hydraulic conductivity (PLC; upper pannels) and photosynthesis (lower panels) in a virtual transplantation experiment along a longitudinal gradient of the population of *H. dactyloides* in Coffs Harbour and of *H. leucoptera* in Dandry with variable LAI. Simulated values of LAI ranged from 100 % of the current LAI to 5% of the current LAI. Note different axis scale in the lower graphs.

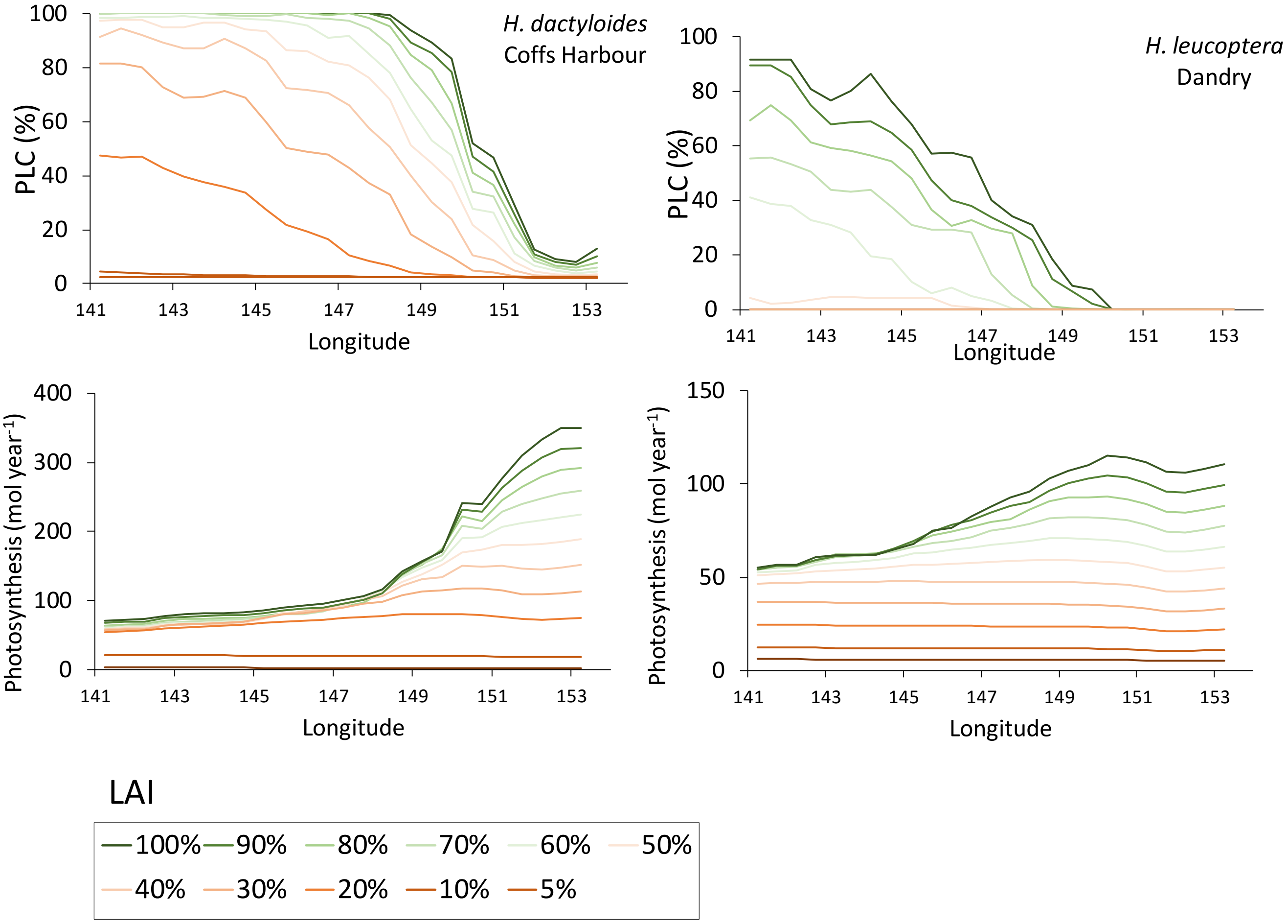

Table S1. Vegetation cover and type, average height of Hakea and soil characteristics of the populations of *Hakea leucoptera* and *Hakea dactyloides* used in the study.

Species	Population	Vegetation type	FC	Height (m)	Soil type	Soil depth (m)	PAWC (mm)	Soil BD (Mg m-3)	Clay (%)
H. leucoptera	Calperum	Chenopod shrublands, samphire shrubs and forblands	28	2	Sodosol	0.7	133	1.50	34.46
H. leucoptera	Opal	Casuarina forests and woodlands	18	2.5	Calcarosol	1.2	144	1.32	31.84
H. leucoptera	Mildura	Eucalyptus woodlands	25	4	Tenosol	1.2	106	1.43	48.81
H. leucoptera	Wilcannia	Eucalyptus woodlands	29	3	Tenosol	1.2	114	1.435	48.81
H. leucoptera	Toorale	Acacia shrublands	40	4.5	Tenosol	0.8	132	1.58	44.20
H. leucoptera	Tilpa	Callitris forests and woodlands	29	5	Tenosol	1.2	144	1.32	31.84
H. leucoptera	Binya	Eucalyptus open woodlands	50	5	Calcarosol	0.7	131	0.97	17.19
H. leucoptera	Kenebri	Eucalyptus open woodlands	59	6	Rudosol	1	58	1.65	29.33
H. leucoptera	Pilliga	Eucalyptus woodlands	68	6	Rudosol	1	58	1.65	39.33
H. leucoptera	Dandry	Callitris forests and woodlands	67	6.5	Rudosol	1.1	150	1.28	25.05
H. dactyloides	Monga	Eucalyptus open forest	72	2.5	Sodosol	1.2	164	1.26	27.44
H. dactyloides	Meryla	Eucalyptus woodlands	67	3.5	Sodosol	1.1	132	1.33	17.03
H. dactyloides	Blue mountains	Eucalyptus woodlands	72	2.5	Sodosol	1.1	71	1.33	17.03
H. dactyloides	Coffs Harbour	Eucalyptus tall open forests	71	3	Sodosol	0.9	59	1.56	45.48

FC- Fractional cover of persistent vegetation. Vegetation type. PAWC water: plant available water capacity. Soil BD: soil bulk density

Table S2. Bioclimatic variables of the populations of *Hakea leucoptera* and *Hakea dactyloides* used in the study. Note that Bio 1: mean annual temperature, Bio 12: mean annual precipitation, Bio 14: precipitation of the driest quarter, Bio 28: Soil moisture index- annual mean, are included in Table 1 of the manuscript. Data from www.ala.org.au

Sp	Population	Bio3	Bio4	Bio9	Bio10	Bio11	Bio15	Bio18	Bio19	Bio29	Bio30	Bio31	Bio34	Bio35
H. leucoptera	Calperum	0.49	1.7	19.6	23.9	11.3	28	52	72	0.41	0.04	70	0.06	0.35
H. leucoptera	Opal	0.46	2.07	13.3	27.3	11.8	21	75	58	0.26	0.05	55	0.07	0.23
H. leucoptera	Mildura	0.48	1.79	20.3	24	10.7	23	61	79	0.47	0.05	67	0.08	0.41
H. leucoptera	Wilcannia	0.45	2.11	13.5	27.7	11.9	24	88	62	0.27	0.05	53	0.08	0.23
H. leucoptera	Toorale	0.44	2.13	16.7	28.1	12.2	23	93	68	0.36	0.08	54	0.09	0.28
H. leucoptera	Tilpa	0.45	2.1	13.66	27.1	11.5	20	97	78	0.38	0.07	57	0.09	0.32
H. leucoptera	Binya	0.45	1.96	20.7	23.7	9.3	14	106	123	0.74	0.11	64	0.14	0.68
H. leucoptera	Kenebri	0.47	2.08	14.3	25.6	10.2	24	179	122	0.65	0.17	47	0.21	0.57
H. leucoptera	Pilliga	0.47	2.07	14	25.9	10.6	26	200	120	0.57	0.14	46	0.19	0.5
H. leucoptera	Dandry	0.47	1.92	11.7	23.6	9.4	24	248	165	0.85	0.23	42	0.32	0.77
H. dactyloides	Monga	0.47	1.57	6.8	17.6	6.2	20	262	192	0.98	0.33	29	0.44	0.96
H. dactyloides	Meryla	0.46	1.51	9.2	19.3	8.2	20	286	242	1	0.3	28	0.48	0.99
H. dactyloides	Blue mountains	0.45	1.54	7.5	18.4	7.1	36	399	195	1	0.5	15	0.7	1
H. dactyloides	Coffs Harbour	0.49	1.37	14.3	23	12.8	44	471	181	1	0.45	24	0.77	0.98

Bio 3: Isothermality; Bio4: Temperature seasonality; Bio9: Mean temperature of the driest quarter; Bio10: Mean temperature of the warmest quarter; Bio11: Mean temperature of the coldest quarter; Bio15: Precipitation seasonality; Bio18: Precipitation of the warmest quarter; Bio19: Precipitation of the coldest quarter; Bio29: Soil moisture index-highest period; Bio30: Soil moisture index-lowest period; Bio31: Soil moisture index seasonality; Bio34: Soil moisture index-warmest quarter mean; Bio35: Soil moisture index-coldest quarter mean.

Parameters used in the simulations with *SurEau*

Table S3. Main physiological parameters of the different tree organs and compartments of *Hakea leucoptera* used in the sensitivity analysis with the model *SurEau* to predict the time to complete hydraulic failure (time to death).

Shrub 4 m high, with a diameter of 3.1cm, and leaf area of 0.66 m^2

Organs	Parameters	Leaf	Branch	Trunk	Root
Symplasm	$\pi 0$ (MPa)	-2.2 / -3.2	-2.2 / -3.2	-2.2 / -3.2	-2.2 / -3.2
	Ɛ (MPa^{-1})	25.5	25.5	25.5	25.5
	K (mmol s^{-1} MPa^{-1})	21.5	218.6	58.7	67.8
	Q_0 (mol)	2.75	14.8	44.4	29.6
	Surface (m^2)	0.66	0.22	0.29	0.34
Apoplasm	P50 (MPa)	-6.9	-6.9	-6.9	-6.9
	Slope (% MPa^{-1})	32.9	32.9	32.9	32.9
	K (mmol s^{-1} MPa^{-1})	21.5	21.9	14	21.9
	Q_0 (mol)	0.91	8.45	24.3	16.9
	C (mmol MPa^{-1})	9.17	84.5	243	169

Table S4. Climatic conditions used in the sensitivity analysis with the model *SurEau* to predict the time to complete hydraulic failure (time to death) of the species *Hakea leucoptera*.

Climatic conditions	$T_{air-min}$ °C	$T_{air-max}$ °C	$RH_{air-min}$ %	$RH_{air-max}$ %	*PAR* µmol	*Wind speed* ms^{-1}	*VPDmax* kPa
Values	20	30	30	80	1500	1.0	3.0

Table S5. Main parameters for the flows in gas phase used in the sensitivity analysis with the model *SurEau* to predict the time to complete hydraulic failure (time to death) of the species *Hakea leucoptera*.

Gas phase Parameters	g_{Stom_max} mmol s^{-1} m^{-2}	g_{Stom_min} mmol s^{-1} m^{-2}	g_{Cuti} mmol s^{-1} m^{-2}	T_{phase} °C	Q10a	Q10b	g_{Crown} mmol s^{-1} m^{-2}
Values	150	5	1.9-5.6	35	1.2	4.8	200

Table S6. Soil parameters used for the sensitivity analysis with the model *SurEau* to predict the time to complete hydraulic failure (time to death) of the species *Hakea leucoptera*.

Soil Parameters	*volume* m^3	*Soil type*	θ_s	θ_r	α cm^{-1}	n	K_{sat} mmol/s/MPa	*l*	Q_{soil0} *mol*
Values	1	clay	0.459	0.098	0.015	1.253	1.69	0.5	25500

Table S7. Main physiological parameters of the different tree organs and compartments of *Hakea dactyloides* used in the sensitivity analysis with the model *SurEau* to predict the time to complete hydraulic failure (time to death).

Shrub 4 m high, with a diameter of 3.6 cm, and leaf area of 3.58 m2.

Organs	Parameters	Leaf	Branch	Trunk	Root
Symplasm	$\pi 0$ (MPa)	-1.5 / -2.5	-1.5 / -2.5	-1.5 / -2.5	-1.5 / -2.5
	ε (MPa^{-1})	16.9	16.9	16.9	16.9
	K (mmol s^{-1} MPa^{-1})	73.6	251.4	67.45	77.9
	Q_0 (mol)	14.9	19.6	58.7	39.1
	Surface (m^2)	3.58	0.25	0.34	0.39
Apoplasm	P50 (MPa)	-4.7	-4.7	-4.7	-4.7
	Slope (% MPa^{-1})	24.8	24.8	24.8	24.8
	K (mmol s^{-1} MPa^{-1})	73.6	76.7	49.1	76.7
	Q_0 (mol)	5.0	11.2	32.2	22.4
	C (mmol MPa^{-1})	49.7	112	322	224

Table S8. Climatic conditions used in the sensitivity analysis with the model *SurEau* to predict the time to complete hydraulic failure (time to death) of the species *Hakea dactyloides*.

Climatic conditions	$T_{air-min}$ °C	$T_{air-max}$ °C	$RH_{air-min}$ %	$RH_{air-max}$ %	*PAR* µmol	*Wind speed* ms^{-1}	*VPDmax* kPa
Values	20	30	30	80	1500	1.0	3.0

Table S9. Main parameters for the flows in gas phase used in the sensitivity analysis with the model *SurEau* to predict the time to complete hydraulic failure (time to death) of the species *Hakea dactyloides*.

Gas phase Parameters	g_{Stom_max} mmol s^{-1} m^{-2}	g_{Stom_min} mmol s^{-1} m^{-2}	g_{Cuti} mmol s^{-1} m^{-2}	T_{phase} °C	Q10a	Q10b	g_{Crown} mmol s^{-1} m^{-2}
Values	150	5	1.2-3.6	35	1.2	4.8	200

Table S10. Soil parameters used for the sensitivity analysis with the model *SurEau* to predict the time to complete hydraulic failure (time to death) of the species *Hakea dactyloides*.

Soil Parameters	*volume* m^3	*Soil type*	θ_s	θ_r	α cm^{-1}	n	K_{sat} mmol/s/MPa	*l*	Q_{soil0} *mol*
Values	1	clay	0.459	0.098	0.015	1.253	1.69	0.5	25500

Table S11. Correlation matrix of climatic variables and traits included in the study for 10 populations of *H. leucoptera*. Acronyms as in Table 2 and Table 2. Numbers in bold indicate significant correlations.

	LAI	MAT	MAP	Pdry	SMI	AI	p12	p50	p88	Ks	Kl	MVL	HV	WD	lma	%C	%N	C:N	d13C	d15N	SWC	RWCTLP	YTLP	Po	CFT	CTLP	CFT*	e	gmin	HSM50	HSM88
LAI	**1.00**																														
MAT	-0.56	**1.00**																													
MAP	**0.87**	-0.49	**1.00**																												
Pdry	**0.84**	-0.50	**0.99**	**1.00**																											
SMI	**0.86**	**-0.78**	**0.90**	**0.92**	**1.00**																										
AI	0.03	0.31	-0.07	0.00	-0.02	**1.00**																									
p12	0.12	-0.04	-0.25	-0.28	-0.07	0.43	**1.00**																								
p50	-0.33	0.12	-0.51	-0.47	-0.32	0.10	0.27	**1.00**																							
p88	-0.28	0.03	-0.15	-0.10	-0.13	-0.39	-0.56	0.61	**1.00**																						
Ks	**0.86**	**-0.64**	**0.88**	**0.88**	**0.90**	-0.01	-0.09	-0.61	-0.38	**1.00**																					
Kl	0.30	-0.11	-0.10	-0.12	0.06	0.36	**0.86**	0.12	-0.56	0.18	**1.00**																				
MVL	**0.63**	-0.56	**0.83**	**0.86**	**0.80**	-0.12	-0.45	-0.63	-0.08	**0.85**	-0.24	**1.00**																			
HV	**-0.73**	0.51	**-0.81**	**-0.82**	**-0.77**	0.12	0.45	0.60	0.11	**-0.89**	0.16	**-0.89**	**1.00**																		
WD	**-0.68**	0.29	**-0.74**	**-0.81**	**-0.74**	-0.34	0.12	0.27	0.13	**-0.79**	-0.16	**-0.71**	**0.74**	**1.00**																	
lma	**-0.72**	0.26	**-0.72**	**-0.74**	**-0.64**	-0.12	0.22	0.45	0.19	**-0.75**	0.03	**-0.73**	**0.85**	**0.78**	**1.00**																
%C	**-0.92**	0.35	**-0.80**	**-0.78**	**-0.76**	-0.26	-0.11	0.35	0.37	**-0.82**	-0.30	-0.55	**0.74**	**0.78**	**0.82**	**1.00**															
%N	**0.90**	-0.27	**0.79**	**0.76**	**0.70**	0.20	0.26	-0.32	-0.42	**0.76**	0.40	0.47	-0.58	**-0.73**	**-0.74**	**-0.93**	**1.00**														
C:N	**-0.90**	0.29	**-0.77**	**-0.75**	**-0.71**	-0.22	-0.26	0.33	0.43	**-0.77**	-0.41	-0.50	0.60	**0.75**	**0.79**	**0.94**	**-0.99**	**1.00**													
d13C	0.27	-0.11	0.02	0.03	0.15	0.50	0.21	-0.13	-0.41	0.30	0.35	0.01	-0.35	-0.28	-0.31	-0.49	0.22	-0.25	**1.00**												
d15N	-0.41	0.42	-0.57	-0.58	-0.51	0.43	0.40	0.44	-0.10	-0.53	0.28	**-0.80**	0.60	0.40	0.61	0.24	-0.31	0.35	0.41	**1.00**											
SWC	**0.93**	-0.52	**0.91**	**0.90**	**0.88**	0.06	-0.09	-0.47	-0.28	**0.95**	0.17	**0.76**	**-0.88**	**-0.83**	**-0.82**	**-0.94**	**0.86**	**-0.87**	0.37	-0.43	**1.00**										
WCTL	-0.03	-0.36	0.18	0.24	0.23	-0.31	**-0.65**	-0.26	0.37	0.26	-0.41	0.59	-0.43	-0.15	-0.05	0.18	-0.34	0.32	-0.11	-0.46	0.10	**1.00**									
YTLP	**0.67**	**-0.72**	**0.77**	**0.73**	0.77	**-0.63**	-0.40	-0.46	0.04	**0.75**	-0.25	**0.75**	**-0.79**	-0.40	-0.58	-0.52	0.47	-0.47	-0.06	**-0.69**	**0.71**	0.34	**1.00**								
Po	0.36	-0.40	**0.65**	0.63	0.53	-0.59	-0.52	-0.37	0.24	0.45	-0.50	**0.65**	-0.50	-0.27	-0.41	-0.18	0.29	-0.28	-0.59	**-0.82**	0.39	0.30	**0.80**	**1.00**							
CFT	0.60	-0.25	0.53	0.45	0.45	-0.21	0.12	-0.07	-0.12	0.36	0.00	0.14	-0.31	-0.23	-0.51	-0.61	**0.68**	**-0.67**	0.01	-0.21	0.51	-0.57	0.54	0.46	**1.00**						
CTLP	**0.69**	-0.51	0.40	0.35	0.51	-0.17	0.39	0.00	-0.24	0.56	**0.65**	0.12	-0.34	-0.36	-0.24	-0.62	0.62	-0.61	0.32	0.02	0.61	-0.19	0.44	0.03	0.43	**1.00**					
CFT*	0.62	-0.33	0.51	0.43	0.49	-0.10	0.32	-0.03	-0.25	0.37	0.17	0.05	-0.20	-0.19	-0.33	-0.61	**0.68**	**-0.66**	0.07	-0.01	0.50	-0.63	0.46	0.31	**0.94**	0.55	**1.00**				
e	-0.45	0.11	-0.38	-0.29	-0.25	0.36	-0.05	0.10	0.07	-0.22	0.06	-0.06	0.24	0.08	0.47	0.46	-0.56	0.55	0.08	0.27	-0.37	0.56	-0.50	-0.48	**-0.95**	-0.34	**-0.82**	**1.00**			
gmin	**0.78**	-0.32	**0.77**	**0.80**	**0.75**	0.40	-0.08	-0.49	-0.37	**0.85**	0.14	**0.72**	**-0.84**	**-0.88**	**-0.87**	**-0.90**	**0.77**	**-0.80**	0.55	-0.33	**0.90**	0.09	0.46	0.16	0.33	0.34	0.30	-0.18	**1.00**	-0.55	
HSM5	0.60	-0.52	**0.76**	**0.71**	**0.66**	-0.43	-0.40	**-0.83**	-0.30	**0.80**	-0.22	**0.81**	**-0.82**	-0.40	-0.61	-0.52	0.47	-0.47	0.03	**-0.67**	**0.70**	0.35	**0.88**	**0.71**	0.38	0.28	0.31	-0.37	0.55	**1.00**	
HSM8	0.61	-0.40	**0.77**	**0.74**	**0.65**	-0.09	-0.24	**-0.93**	-0.54	**0.84**	-0.07	**0.82**	**-0.79**	-0.51	-0.62	-0.58	0.53	-0.54	0.16	-0.55	**0.73**	0.30	**0.68**	0.51	0.23	0.21	0.22	-0.18	**0.69**	**-0.92**	**1.00**

Table S12. Correlation matrix of climatic variables and traits included in the study for 4 populations of *H. dactyloides*. Acronyms as in Table 2 and Table 2. Numbers in bold indicate significant correlations.

	LAI	MAT	MAP	Pdry	SMI	AI	p12	p50	p88	Ks	Kl	MVL	HV	WD	Ima	%C	%N	C:N	d13C	d15N	SWC	RWCTLP	YTLP	Po	CFT	CTLP	CFT*	e	gmin	HSM50	HSM88
LAI	**1.00**																														
MAT	0.12	**1.0**																													
MAP	-0.49	0.8	**1.00**																												
Pdry	-0.06	-0.7	-0.64	**1.00**																											
SMI	**-0.98**	0.1	0.64	-0.08	**1.00**																										
AI	-0.80	-0.3	0.16	0.60	0.74	**1.00**																									
p12	-0.07	**1.0**	0.89	-0.63	0.25	-0.10	**1.00**																								
p50	-0.29	0.1	0.22	0.55	0.32	0.72	0.30	**1.00**																							
p88	-0.88	-0.5	0.08	0.51	0.79	0.94	-0.30	0.43	**1.00**																						
Ks	0.94	-0.2	-0.76	0.26	**-0.98**	-0.61	-0.38	-0.22	-0.67	**1.00**																					
Kl	-0.14	**-1.0**	-0.79	0.83	-0.04	0.43	-0.94	0.04	0.55	0.21	**1.00**																				
MVL	-0.10	-0.9	-0.78	0.93	-0.08	0.49	-0.87	0.22	0.54	0.26	**0.98**	**1.00**																			
HV	**-0.99**	-0.1	0.53	-0.06	**0.98**	0.71	0.09	0.18	0.83	**-0.96**	0.08	0.01	**1.00**																		
WD	0.72	-0.6	**-0.96**	0.56	-0.83	-0.33	-0.69	-0.16	-0.33	0.92	0.58	0.61	-0.77	**1.00**																	
Ima	-0.46	-0.2	0.13	-0.43	0.42	-0.07	-0.25	-0.71	0.26	-0.47	0.11	-0.10	0.56	-0.36	**1.00**																
%C	-0.14	**-1.0**	-0.78	0.86	-0.04	0.46	-0.92	0.10	0.56	0.22	**1.00**	**0.99**	0.07	0.58	0.04	**1.00**															
%N	-0.18	**-1.0**	-0.75	0.62	0.00	0.29	**-0.97**	-0.24	0.51	0.14	**0.95**	0.87	0.16	0.50	0.38	0.93	**1.00**														
C:N	0.16	**1.0**	0.77	-0.64	0.03	-0.29	**0.97**	0.22	-0.50	-0.16	**-0.96**	-0.88	-0.13	-0.52	-0.35	-0.94	**-1.00**	**1.00**													
d13C	0.35	-0.9	**-0.98**	0.78	-0.51	0.05	-0.90	-0.05	0.11	0.65	0.88	0.89	-0.41	0.90	-0.17	0.88	0.80	-0.82	**1.0**												
d15N	0.02	0.8	0.73	**-0.99**	0.13	-0.53	0.72	-0.44	-0.48	-0.32	-0.88	**-0.96**	0.09	-0.63	0.36	-0.91	-0.70	0.72	-0.9	**1.00**											
SWC	-0.87	0.4	0.84	-0.40	0.94	0.49	0.50	0.17	0.54	**-0.99**	-0.36	-0.41	0.90	**-0.97**	0.46	-0.37	-0.28	0.30	-0.8	0.46	**1.00**										
RWCTL	-0.04	-0.8	-0.73	**0.99**	-0.11	0.54	-0.74	0.42	0.50	0.30	0.90	0.97	-0.07	0.62	-0.33	0.92	0.72	-0.74	0.9	**-1.00**	-0.45	**1.00**									
YTLP	**-0.96**	0.2	0.73	-0.18	**0.99**	0.68	0.36	0.30	0.72	**-1.00**	-0.16	-0.19	**0.96**	-0.89	0.41	-0.16	-0.11	0.14	-0.6	0.24	**0.97**	-0.22	**1.00**								
Po	**-0.97**	0.1	0.68	-0.06	**0.99**	0.76	0.32	0.40	0.78	**-0.98**	-0.09	-0.11	**0.96**	-0.85	0.33	-0.09	-0.08	0.10	-0.5	0.13	0.94	-0.12	**0.99**	**1.00**							
CFT	-0.43	0.8	**0.99**	-0.62	0.59	0.15	0.93	0.29	0.03	-0.70	-0.81	-0.79	0.46	-0.91	0.02	-0.81	-0.80	0.82	**-1.0**	0.71	0.79	-0.71	0.68	0.64	**1.00**						
CTLP	-0.19	0.9	0.93	-0.86	0.36	-0.22	0.92	-0.05	-0.27	-0.52	-0.94	**-0.95**	0.26	-0.81	0.15	-0.95	-0.85	0.86	**-1.0**	0.91	0.65	-0.92	0.47	0.39	0.93	**1.00**					
CFT*	-0.36	0.9	**0.98**	-0.77	0.52	-0.03	0.91	0.08	-0.09	-0.66	-0.87	-0.88	0.41	-0.90	0.16	-0.88	-0.80	0.82	**-1.0**	0.84	0.77	-0.84	0.62	0.55	**0.98**	**0.98**	**1.0**				
e	0.58	-0.7	**-0.99**	0.65	-0.72	-0.19	-0.81	-0.15	-0.16	0.82	0.72	0.74	-0.63	**0.98**	-0.26	0.73	0.65	-0.67	**1.0**	-0.73	-0.90	0.72	-0.79	-0.74	**-0.97**	-0.91	**-1.0**	**1.00**			
gmin	-0.21	0.9	**0.94**	-0.84	0.39	-0.18	0.92	-0.01	-0.25	-0.54	-0.93	-0.94	0.28	-0.83	0.13	-0.94	-0.85	0.87	**-1.0**	0.90	0.67	-0.90	0.49	0.42	0.94	**1.00**	**1.0**	-0.92	**1.00**		
HSM5	-0.48	0.0	0.37	-0.63	0.49	-0.12	0.01	-0.67	0.17	-0.58	-0.15	-0.35	0.59	-0.56	**0.96**	-0.21	0.13	-0.09	-0.4	0.58	0.61	-0.55	0.51	0.42	0.27	0.41	0.4	-0.49	0.39	**1.00**	
HSM8	0.00	-0.1	-0.03	-0.60	-0.01	-0.52	-0.23	**-0.95**	-0.20	-0.08	-0.05	-0.25	0.13	-0.10	0.88	-0.12	0.25	-0.23	-0.1	0.50	0.12	-0.48	0.00	-0.10	-0.12	0.16	0.1	-0.07	0.13	-0.86	**1.00**

Table S13. Percentage of the explained variation and significance values (ns non-significant; *p<0.05; **p<0.01; ***p<0.001) due to species and population within species for ten populations of *H. leucoptera* and four populations of *H. dactyloides*.

Trait	Species	Population
Stem traits		
P_{12}	93.79***	2.51**
P_{50}	93.20***	0.55*
P_{88}	84.39***	4.06**
Ks	76.20***	6.95***
Kl	39.85***	3.17^{ns}
MVL	76.25***	11.50***
HV	58.84***	28.37***
WD	51.05***	23.48***
Foliar traits		
LMA	86.56***	11.86***
%C	34.57***	37.27***
%N	2.51***	63.26***
C:N	4.38***	65.57***
$\delta^{13}C$	85.23***	2.12**
$\delta^{15}N$	0^{ns}	94.75***
SWC	72.73***	16.89***
RWC_{TLP}	41.36***	19.02***
Ψ_{TLP}	79.49***	8.45***
Π_o	55.08***	7.33**
C_{FT}	63.12***	10.25**
C_{FT}*	50.36***	19.47***
C_{TLP}	71.88***	6.68***
ε	39.10***	21.97***
g_{min}	15.55***	42.92***
Hydraulic safety margins		
HSM_{50}	82.88***	7.51***
HSM_{88}	67.74***	21.74***

P_{12}: Xylem pressure at 12% loss of hydraulic conductivity; P_{50}: Xylem pressure at 50% loss of hydraulic conductivity; P_{88}: Xylem pressure at 88% loss of hydraulic conductivity; K_s: Xylem specific conductivity; K_l: Leaf specific conductivity; MVL: Maximum vessel length; HV: Huber value; WD: Wood density; LMA: Leaf mass per area; %C: Carbon content; %N: Nitrogen content; $\delta^{13}C$: Carbon isotope signature; $\delta^{15}N$: Nitrogen isotope signature; SWC: Saturated water content; RWC_{TLP}: Relative water content at turgor loss point; Ψ_{TLP}: Turgor loss point; Π_o: Osmotic potential at full turgor; C_{FT}: Capacitance at full turgor; C_{FT}*: Absolute capacitance at full turgor; C_{TLP}: Capacitance after turgor loss point; ε: Modulus of elasticity; g_{min}: Minimum epidermal conductance; HSM_{50}: Hydraulic safety margin at 50% loss of conductivity; HSM_{88}: Hydraulic safety margin at 88% loss of conductivity.

Table S14. Loadings of the stem and leaf traits of the first five Principal components in the Principal Component Analysis (PCA). All variables were equally weighted in the analysis.

Trait	**Factor 1**	**Factor 2**	**Factor 3**	**Factor 4**	**Factor 5**
P_{50}	0.94	-0.23	0.08	0.10	0.19
Ks	0.90	0.26	-0.02	0.18	0.14
Kl	-0.85	0.18	0.29	-0.09	0.21
HV	-0.77	-0.52	0.14	-0.26	0.07
WD	-0.79	-0.41	-0.18	-0.27	0.07
LMA	-0.91	-0.31	0.01	-0.12	-0.12
%C	0.48	-0.82	-0.27	0.05	0.03
%N	-0.21	0.86	0.21	-0.21	0.30
$\delta^{13}C$	-0.98	0.16	-0.05	-0.04	0.02
$\delta^{15}N$	-0.11	-0.52	0.79	0.10	-0.21
RWC_{TLP}	-0.92	0.16	-0.12	0.27	0.01
Ψ_{TLP}	0.95	0.18	-0.12	-0.02	-0.07
Π_o	0.91	0.14	-0.29	-0.14	-0.09
C_{FT}	0.92	0.13	0.22	-0.23	-0.10
C_{TLP}	0.92	0.00	0.28	0.03	-0.12
ε	-0.79	-0.23	-0.13	0.51	0.02
g_{min}	-0.34	0.87	0.16	0.25	-0.12
HSM_{50}	0.68	-0.53	0.23	0.18	0.38

P_{50}: Xylem pressure at 50% loss of hydraulic conductivity; K_s: Xylem specific conductivity; K_l: Leaf specific conductivity; HV: Huber value; WD: Wood density; LMA: Leaf mass per area; %C: Carbon content; %N: Nitrogen content; $\delta^{13}C$: Carbon isotope signature; $\delta^{15}N$: Nitrogen isotope signature; RWC_{TLP}: Relative water content at turgor loss point; Ψ_{TLP}: Turgor loss point; Π_o: Osmotic potential at full turgor; C_{FT}: Capacitance at full turgor; C_{TLP}: Capacitance after turgor loss point; ε: Modulus of elasticity; g_{min}: Minimum epidermal conductance; HSM_{50}: Hydraulic safety margin at 50% loss of conductivity.